ACS APPLIED MATERIALS & INTERFACES

Research Article

www.acsami.org

Steady-State and Femtosecond Transient Absorption Spectroscopy of New Two-Photon Absorbing Fluorene-Containing Quinolizinium Cation Membrane Probes

Xiling Yue,[†] Zach Armijo,[†] Kevan King,[†] Mykhailo V. Bondar,[‡] Alma R. Morales,[†] Andrew Frazer,[†] Ivan A. Mikhailov,[§] Olga V. Przhonska,[‡] and Kevin D. Belfield*[,†,∇,∥]

[†]Department of Chemistry, University of Central Florida, P.O. Box 162366, Orlando, Florida 32816, United States

[‡]Institute of Physics, National Academy of Sciences, Prospect Nauki 46, Kiev, 03028, Ukraine

[§]Petersburg Nuclear Physics Institute, 188300, St. Petersburg, Russia

[∇]School of Chemistry and Chemical Engineering, Shaanxi Normal University, Xi'an, 710062, People's Republic of China

[∥]College of Science and Liberal Arts, New Jersey Institute of Technology, University Heights, Newark, New Jersey 07102, United States

Supporting Information

ABSTRACT: The synthesis, linear photophysical characterization, and nonlinear optical properties of two new symmetrical fluorene-containing quinolizinium derivatives, 2,8-bis((E)-2-(7-(diphenylamino)-9,9-dihexyl-9H-fluoren-2-yl)-vinyl)quinolizinium hexafluorophosphate (**1**) and 2,8-bis((E)-2-(7-((7-(diphenylamino)-9,9-dihexyl-9H-fluoren-2-yl)-ethynyl)-9,9-dihexyl-9H-fluoren-2yl)vinyl)quinolizinium hexafluorophosphate (**2**), are reported. The nature of the dual-band steady-state fluorescence emission of **1** and **2** was determined, and violation of Kasha's rule along with a strong dependence on solvent polarity were shown. A relatively complex structure of two-photon absorption (2PA) spectra of **1** and **2**, with maximum cross sections of ∼400−600 GM, was determined using the open aperture Z-scan method. Different types of fast relaxation processes with characteristic times of 0.3−0.5 ps and 1.5−2 ps were observed in the excited states of the new compounds via femtosecond transient absorption pump−probe spectroscopy. To better understand the photophysical behavior of **1** and **2**, a quantum-mechanical study was undertaken using TD-DFT and ZINDO/S methods. Simulated linear absorption spectra were found to be in good agreement with experimental data, while 2PA cross sections were overestimated. Although the new dyes were highly fluorescent in nonpolar solvents, they were essentially nonfluorescent in polar media. Significantly, the quinolizinium dyes exhibited fluorescence turn-on behavior upon binding to bovine serum album (BSA) protein, exhibiting over 4-fold fluorescence enhancement, which was a finding that was leveraged to demonstrate cell membrane fluorescence imaging of HeLa cells.

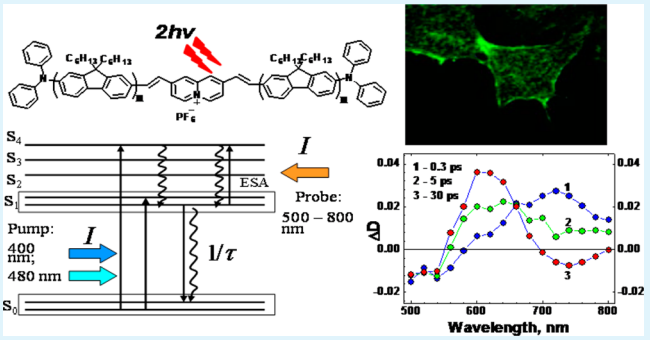

KEYWORDS: *quinolizinium derivatives, fluorescence probes, two-photon absorption, femtosecond transient absorption spectroscopy, fluorescence bioimaging*

1. INTRODUCTION

Heteroatomic cations are widely employed in many areas of applications, including chemical synthesis,[1,2] metal ion detection,[3,4] photodynamic therapy,[5−7] optical power limiting,[8−10] and one- and two-photon fluorescence bioimaging microscopy.[11−13] The use of cationic structures as a fluorescent probe, in turn, is concerned with various biomedical techniques, such as fluorimetric detection of DNA and proteins[14−16] and efficient staining agents of organelles in the cytoplasm[17,18] Such applications are based on fundamental linear photophysical and nonlinear optical properties of the charged organic molecules, including fast dynamic processes in the ground and excited electronic states.[19−21] One of the most intriguing types of a cationic structure is a quinolizinium derivative with general D-π-A^+ and D-π-A^+-π-D molecular architectures,[11,22] where A^+ is a charged cationic electron-deficient core and D represents electron-donating substituents. A new V-shaped quinolizinium derivative of this type, (*E*,*E*)-2,8-bis(4-*N*,*N*-dimethylaminophenylvinyl) quinolizinium hexafluorophosphate (V-DMA2), was shown as a promising marker for fluorescence microscopy of live cells, exhibiting a large two-photon absorption (2PA) cross

Received: November 18, 2014
Accepted: January 13, 2015
Published: January 26, 2015

DOI: 10.1021/am508093p
ACS Appl. Mater. Interfaces 2015, 7, 2833−2846

Scheme 1. Synthesis of Bis-Fluorenyl Quinolizinium (1)

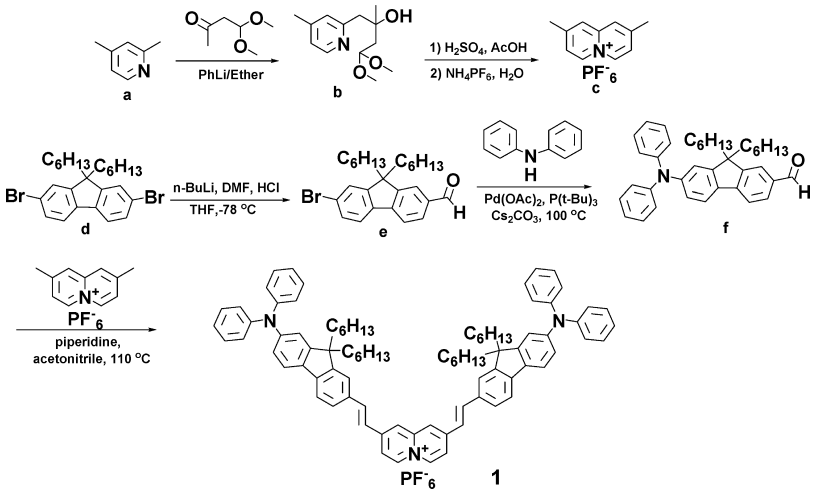

Scheme 2. Synthesis of Tetra-Fluorenyl Quinolizinium (2)

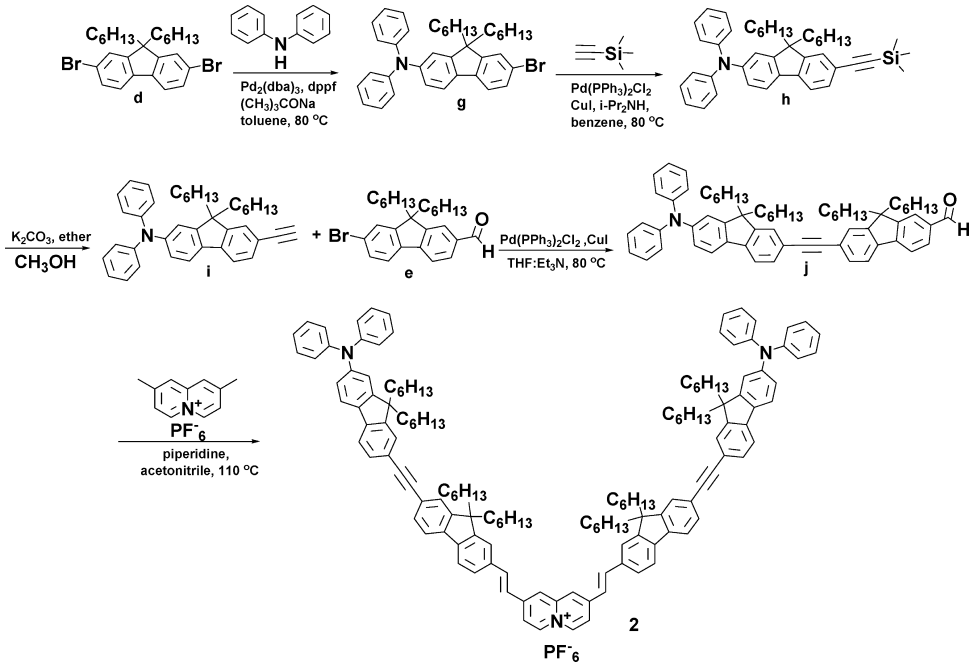

section and dramatic increase in fluorescence intensity upon binding to DNA.[11]

Linear spectroscopic and excited-state deactivation processes of a series of benzo[*b*]quinolizinium derivatives were reported as highly sensitive "light-up" fluorescent probes for DNA and protein detection.[4,15,16,23] The nature of ultrafast relaxations in the excited state of naphto[1,2-*b*]quinolizinium bromide and its interaction with DNA were probed by femtosecond transient absorption spectroscopy.[24] It is worth mentioning that fast relaxations in the excited state of quinolizinium derivatives are scarcely addressed in the scientific literature; therefore, this is a subject of keen interest, as is increasing their 2PA efficiency, which is a challenging task.

In this paper, the synthesis and comprehensive investigation of linear spectroscopic, photochemical, and nonlinear optical properties of new fluorene-containing quinolizinium derivatives 2,8-bis((E)-2-(7-(diphenylamino)-9,9-dihexyl-9H-fluoren-2-yl)-vinyl)quinolizinium hexafluorophosphate (**1**) and 2,8-bis((E)-2-(7-((7-(diphenylamino)-9,9-dihexyl-9H-fluoren-2-yl)-ethynyl)-9,9-dihexyl-9H-fluoren-2-yl)vinyl)quinolizinium hexafluorophosphate (**2**) are reported, including 2PA and femtosecond transient absorption spectroscopy analysis. The newly synthesized compounds **1** and **2** were also investigated theoretically: density functional theory (DFT) was used for the geometry optimization, while time-dependent density functional theory (TD-DFT) and ZINDO/S[25,26] were used for the simulation of the excited states. Potential uses of the new probes were explored, resulting in turn-on fluorescence behavior upon binding to BSA in an aqueous medium.

2. EXPERIMENTAL SECTION

2.1. Synthetic Strategy. Schemes 1 and 2 (shown below) depict the synthesis of quinolizinium dyes **1** and **2**, respectively. The use of a double substitution strategy enabled the synthesis of these charged 2D V-shaped chromophores, based on a D-π-A^+-π-D noncentrosymmetric architecture, fabricated on the charged heterocyclic quinolizinium cation (A^+), as an acceptor unit and diphenylaminofluorene and

DOI: 10.1021/am508093p
ACS Appl. Mater. Interfaces 2015, 7, 2833−2846

diphenylamino bisfluorenylyne (fluorenes bridged by an alkyne) as donors. Both chromophores began with the reported synthesis of the dimethylquinolizinium cation, which was achieved by 2-methyl lithiation of 2,4-lutidine succeeded by reaction with phenyllithium using dry Et_2O.[1] The addition of 4,4-dimethoxybutan-2-one to this mixture resulted in the formation of hydroxy-acetal (**b**). An acid-catalyzed dehydration reaction realized the cyclization of this product to the corresponding dimethylquinolizinium derivative, which was isolated as its hexafluorophosphate salt (**c**) and characterized by its symmetrical ^{1}H NMR spectrum. Dibromofluorene (**d**) was converted to 7-bromo-9,9-dihexylfluorene-2-carboxaldehyde (**e**) via addition of a stoichiometric amount of *n*-BuLi, followed by reaction with dimethylformamide (DMF).[27] This was followed by the Pd-catalyzed Buchwald–Hartwig arylamination coupling with diphenylamine in toluene to provide 7-(diphenylamino)-9,9-dihexyl-9H-fluorene-2-carbaldehyde (**f**), the precursor to quinolizinium chromophore **1**, using $Pd(OAc)_2$, $P(t\text{-}Bu)_3$, and Cs_2CO_3 (a non-nucleophilic base) in toluene. A double Knoevenagel condensation with the active methyl groups of the 2,8-dimethylquinolizinium hexafluorophosphate (**c**) and 7-(diphenylamino)-9,9-dihexyl-9H-fluorene-2-carbaldehyde (**f**) was conducted in the presence of piperidine in acetonitrile, providing 2,8-bis((E)-2-(7-(diphenylamino)-9,9-dihexyl-9H-fluoren-2-yl)vinyl)-quinolizinium hexafluorophosphate (**1**) as dark-red solid in 30% yield (Scheme 1).

Quinolizinium **2** was synthesized by first employing a Pd-catalyzed arylamination, using diphenylamine and 2,7-dibromo-9,9-dihexylfluorene (**d**) in toluene.[28] The resulting diphenylaminofluorenyl bromide (**g**) then underwent Sonogashira cross-coupling, carried out in benzene with trimethylsilylacetylene, 10 mol % CuI, and 5 mol % $PdCl_2(PPh_3)_2$ with diisopropylamine as a base. These conditions yielded the trimethylsilylalkynylfluorene derivative (**h**), which was subsequently deprotected with K_2CO_3 in CH_3OH affording the ethynylfluorene derivative (**i**). An analogous Sonogashira reaction in THF was then employed to couple this derivative with 7-bromo-9,9-dihexylfluorene-2-carboxaldehyde (**e**), providing 7-((7-(diphenylamino)-9,9-dihexyl-9H-fluoren-2-yl)ethynyl)-9,9-dihexyl-9H-fluorene-2-carbaldehyde (**j**), the precursor to **2**, in 60% yield. The double Knoevenagel condensation of (7-((7-(diphenylamino)-9,9-dihexyl-9H-fluoren-2-yl)ethynyl)-9,9-dihexyl-9H-fluorene-2-carbaldehyde) (**j**) with 2,8-dimethylquinolizinium hexafluorophosphate (**c**) produced 2,8-bis((E)-2-(7-((7-(diphenylamino)-9,9-dihexyl-9H-fluoren-2-yl)-ethynyl)-9,9-dihexyl-9H-fluoren-2-yl)vinyl)quinolizinium hexafluorophosphate (**2**) as red-solid in 35% yield (Scheme 2).

Chromophores **1** and **2** were both found to be soluble in many organic solvents, although chromophore **2** generally exhibited higher solubility, and likely associated with the presence of more alkyl groups present in **2**. This led to a greater ease of purification of both compounds, which is a factor that led to fair yields. During the coupling reactions of **1** and **2**, evidence of the corresponding homocoupled quinolizinium was observed but no further characterization was performed on the monosubstituted species.

2.2. Materials and Methods. Chemicals were purchased from Aldrich and Acros Chemical and used without any further purification unless otherwise stated. Piperidine was dried over Na, distilled under reduced pressure, and stored over 4 Å molecular sieves. Pd-catalyzed reactions were performed in high-pressure Schlenk tubes under N_2. 2,4-Dimethylpyridine (**a**) and 2,7-dibromo-9,9-dihexylfluorene (**d**) were purchased from Aldrich. 3-Hydroxy-3-methyl-4-[2-(4-methylpyridyl)]butanal dimethyl acetal (**b**) and 2,8-dimethylquinolizinium hexafluorophosphate (**c**) were prepared according to procedures reported in the literature.[1] 7-Bromo-9,9-dihexyl-*N*,*N*-diphenyl-9H-fluoren-2-amine (**g**) was synthesized as previously reported.[28] Physical characterization was conducted on all new compounds by ^{1}H and ^{13}C NMR spectroscopy, high-resolution mass spectroscopy (HRMS), and melting point (mp).

*Synthesis of 7-Bromo-9,9-dihexylfluorene-2-carboxaldehyde (**e**).* To a solution containing 2,7-dibromo-9,9-dihexylfluorene (**d**) (20.0 g; 40.6 mmol) in anhydrous THF (120 mL) at −78 °C was added *n*-butyl lithium in hexane (25.3 mL; 1.6 M) dropwise. The reaction was stirred for 1.5 h, followed by the dropwise addition of anhydrous DMF (4.47 mL) stirred at this temperature for 2 h before it was allowed to reach ambient temperature and quenched with H_2O (125 mL). The solution was then stirred for 1 h more and the product was extracted with toluene (100 mL × 2) and dried over anhydrous Na_2SO_4. The crude product was purified by flash chromatography on silica gel using a 10:1 hexanes:ethyl acetate mixture as eluent to yield a yellow solid. Yield: 60% (10.74 g); mp: 41 °C. ^{1}H NMR (400 MHz, $CDCl_3$) δ: 10.02–10.11 (1H, s), 7.75–7.92 (3H, m), 7.57–7.69 (1H, m), 7.45–7.57 (2H, m), 1.87–2.11 (4H, qdd, J = 13.5, 10.9, 5.5), 1.21–1.33 (1H, m), 0.91–1.20 (13H, m), 0.79–0.95 (1H, m), 0.68–0.83 (6H, t, J = 7.1), 0.47–0.67 (4H, m). ^{13}C NMR (101 MHz, $CDCl_3$) δ: 192.22, 154.27, 151.16, 146.35, 138.56, 135.61, 130.57, 130.44, 126.47, 123.10, 122.25, 120.10, 55.62, 40.11, 31.44, 29.53, 23.70, 22.53, 13.96. HR-MS (ESI) calcd for $C_{26}H_{33}BrO$ $[M]^+$, 440.1715; found for $C_{26}H_{33}BrO$ $[M]^+$, 440.1716.

*Synthesis of 7-(Diphenylamino)-9,9-dihexyl-9H-fluorene-2-carbaldehyde (**f**).* Under a nitrogen atmosphere, a mixture of 7-bromo-9,9-dihexyl-9H-fluorene-2-carbaldehyde (**e**) (3.5 g, 7.92 mmol), diphenylamine (2.0 g, 11.87 mmol), $Pd(OAc)_2$ (0.043 g, 0.19 mmol), $P(t\text{-}Bu)_3$ (86 mg, 0.42 mmol), and Cs_2CO_3 (3.86 g, 11.84 mmol) in dry toluene (20 mL) was stirred and heated for 48 h at 120 °C. After cooling to room temperature, the reaction mixture was passed through a short Celite plug, and the filtered solution was concentrated to afford yellow-brown oil. Purification was carried out by flash column chromatography using silica gel as the stationary phase, first hexanes, then 1:1 hexanes/CH_2Cl_2. A yellow solid was obtained; yield: 88% (3.7 g); mp: 39.6–40.2 °C. ^{1}H NMR (500 MHz, $CDCl_3$) δ: 9.69 (s, 1H), 7.50 (dd, J = 7.5 Hz, 2H), 7.40 (dd, J = 8 Hz, 1H), 7.30 (dd, J = 8.5 Hz, 1H), 6.97–6.93 (m, 4H), 6.81 (dd, J = 6.5 Hz, 4H), 6.77 (d, J = 2 Hz, 1H), 6.74–6.71 (m, 4H), 1.72- 1.65 (m, 2H), 1.61–1.53 (m, 2H), 0.02 (t, J = 14.5, 6H). ^{13}C NMR (125 MHz, $CDCl_3$) δ: 192.5, 153.8, 151.4, 149.0, 147.8, 134.6, 134.2, 131.0, 129.4, 124.5, 123.3, 122.9, 121.9, 119.3, 118.4, 55.3, 40.2, 31.7, 29.7, 23.9, 22.7, 14.2. HR-MS (ESI) calcd for $C_{38}H_{43}NO$ $[M]^+$, 529.3339; calcd for $[M + Na]^+$ = 552.3242, found for $[M + Na]^+$, 552.3237.

*Synthesis of 2,8-Bis((E)-2-(7-(diphenylamino)-9,9-dihexyl-9H-fluoren-2-yl)vinyl)quinolizinium hexafluorophosphate (**1**).* 2,8-Dimethylquinolizinium hexafluorophosphate (**c**) (0.25 g, 0.83 mmol) and 7-(diphenylamino)-9,9-dihexyl-9H-fluorene-2-carbaldehyde (**f**) (0.87 g, 1.64 mmol) was added piperidine (0.28 g, 3.3 mmol) in acetonitrile (25 mL) and refluxed for 24 h using a Dean–Stark apparatus. After cooling to ambient temperature, the solvent was removed under reduced pressure. Purification was carried out by column chromatography, first using 4:1 ethyl acetate/hexanes, and then 4:1 CH_2Cl_2/acetonitrile. The pure compound was isolated as a dark red solid; yield: 30% (0.29 g); mp: 130.5–131 °C. ^{1}H NMR (400 MHz, $CDCl_3$) δ: 8.77 (d, J = 7.3 Hz, 1H), 8.00 (d, J = 2.0 Hz, 1H), 7.80 (dd, J = 7.3, 1.9 Hz, 1H), 7.64–7.45 (m, 6H), 7.29 (d, J = 2.0 Hz, 1H), 7.26 (d, J = 2.0 Hz, 1H), 7.18 (s, 1H), 7.16 (d, J = 1.3 Hz, 2H), 7.14 (q, J = 0.9 Hz, 3H), 7.08–6.99 (m, 4H), 3.14 (q, J = 7.3 Hz, 10H), 2.08–1.76 (m, 7H), 1.37 (t, J = 7.3 Hz, 14H), 1.25–0.99 (m, 16H), 0.80 (t, J = 7.0 Hz, 7H), 0.76–0.61 (m, 3H). ^{13}C NMR (126 MHz, $CDCl_3$) δ: 153.0, 151.7, 148.2, 147.7, 145.9, 143.9, 143.1, 140.3, 135.5, 134.8, 132.7, 129.2, 127.8, 124.2, 123.1, 122.9, 122.2, 122.0, 121.1, 120.9, 119.6, 119.0, 118.6, 55.2, 40.1, 31.6, 31.6, 29.7, 29.6, 29.6, 23.9, 22.7, 22.5, 22.5, 14.1, 14.0. HR-MS (MALDI-DTL) calcd for $C_{87}H_{94}N_3$ $[M]^+$, 1180.7442; found for $C_{87}H_{94}N_3$ $[M]^+$, 1180.7457.

*Synthesis of 7-Ethynyl-9,9-dihexyl-N,N-diphenyl-9H-fluoren-2-amine (**i**).* To a solution of 7-bromo-9,9-dihexyl-*N*,*N*-diphenyl-9*H*-fluoren-2-amine (**g**) (4.00 g; 6.90 mmol) in benzene (30 mL) was added $PdCl_2(PPh_3)_2$ (0.29 g; 0.42 mmol), CuI (0.13 g; 0.69 mmol), *i*-Pr_2NH (4.20 g; 41 mmol), and trimethylsilyl acetylene (2.14 g; 22 mmol). This was stirred at 80 °C under a dry nitrogen atmosphere for 30 h. After cooling to ambient temperature, the saturated NH_4Cl solution (50 mL) was added into the reaction mixture, and the resultant solution was stirred at room temperature for 0.5 h. The above solution was extracted with ethyl acetate (30 mL × 3) and filtered through Celite to further remove the remaining catalyst, then dried over $MgSO_4$, and then concentrated under reduced pressure. Compound (**h**) was deprotected without further purification: A

DOI: 10.1021/am508093p
ACS Appl. Mater. Interfaces 2015, 7, 2833–2846

mixture of compound (**h**) (3.71 g; 6.21 mmol), potassium carbonate (1.66 g; 12.08 mmol), ethyl ether (20 mL), and methanol (20 mL) was stirred under a dry nitrogen atmosphere at room temperature for 8 h. Saturated NH_4Cl solution (50 mL) was then added to the reaction mixture, and the mixture was stirred at room temperature for 0.5 h. This was then extracted with ethyl acetate (30 mL × 3) and then dried over $MgSO_4$. All volatiles were removed to reveal the crude product, which was purified through column chromatography on silica gel using hexane/DCM (6:1) as the eluent. The purified product was isolated as a pale-yellow oil. Yield: 94% (3.06 g). ^{1}H NMR (400 MHz, $CDCl_3$) δ: 7.59−7.38 (m, 5H), 7.33−7.20 (m, 6H), 7.17−6.99 (m, 10H), 4.78 (s, 1H), 3.14 (s, 1H), 1.94−1.74 (m, 5H), 1.59 (s, 3H), 1.25−0.95 (m, 16H), 0.82 (td, J = 7.1, 2.1 Hz, 8H), 0.68−0.61 (m, 4H). ^{13}C NMR (101 MHz, $CDCl_3$) δ: 152.5, 150.6, 147.9, 147.7, 141.7, 135.2, 131.2, 129.2, 126.3, 124.0, 123.9, 123.3, 122.7, 122.6, 120.8, 120.4, 119.3, 119.1, 119.0, 118.9, 84.9, 77.3, 77.0, 76.8, 76.7, 55.1, 40.2, 31.5, 29.6, 29.6, 23.7, 22.6, 14.0. HR-MS (ESI) calcd for $C_{39}H_{43}N$ $[M]^+$, 525.3396; found for $C_{39}H_{43}N$ $[M]^+$, 525.3403.

*Synthesis of 7-((7-(Diphenylamino)-9,9-dihexyl-9H-fluoren-2-yl)-ethynyl)-9,9-dihexyl-9H-fluorene-2-carbaldehyde (**j**).* To a solution of 7-ethynyl-9,9-dihexyl-*N*,*N*-diphenyl-9H-fluoren-2-amine (**i**) (1.78 g, 3.39 mmol) in THF:triethylamine (50:50) (30 mL), we added CuI (16 mg; 0.84 mmol) and $Pd(PPh_3)_2Cl_2$ (0.051 g; 0.074 mmol). 7-Bromo-9,9-dihexyl-9H-fluorene-2-carbaldehyde (**e**) (1.0 g; 2.26 mmol) in THF (20 mL) was then added to the mixture. The resultant slurry was then heated at 80 °C for 24 h. The reaction mixture was allowed to cool to room temperature before filtering it through Celite. The Celite cake was then washed with THF (30 mL × 2). The combined filtrates had all volatiles removed under a reduced vacuum to yield a crude yellow oil. Purification of this product was then performed using a silica gel column and eluted with hexane/CH_2Cl_2 (3:1) with 1% triethylamine. The isolated yellow oil was subject to constant vacuum over a period of 24 h to yield a yellow solid. Yield: 60% (1.21 g). mp: 114 °C. ^{1}H NMR (400 MHz, $CDCl_3$) δ: 10.02−10.11 (1H, s), 7.73−7.92 (4H, m), 7.45−7.66 (6H, m), 7.19−7.32 (6H, m), 7.09−7.16 (5H, d, J = 7.8), 6.96−7.07 (3H, m), 1.77−2.14 (8H, m), 1.50−1.59 (2H, s), 0.91−1.20 (24H, ddtt, J = 23.7, 19.7, 9.1, 5.4), 0.72−0.85 (12H, dt, J = 17.2, 7.1), 0.47−0.70 (8H, m). ^{13}C NMR (101 MHz, $CDCl_3$) δ: 192.0, 154.3, 152.5, 152.2, 151.8, 151.1, 150.7, 147.9, 147.7, 146.8, 146.3, 141.5, 139.5, 138.5, 135.7, 135.4, 130.8, 130.5, 130.4, 129.2, 126.5, 126.1, 125.8, 124.0, 123.7, 123.4, 123.1, 122.7, 122.2, 120.9, 120.8, 120.1, 118.9, 91.9, 90.1, 55.6, 55.4, 55.1, 40.1, 31.4, 29.5, 23.7, 22.5, 14.0. HR-MS (MALDI-DTL) calcd for $C_{65}H_{75}NO$ $[M]^+$, 885.5849; found for $C_{65}H_{75}NO$ $[M]^+$, 885.5838.

*Synthesis of 2,8-bis((E)-2-(7-((7-(diphenylamino)-9,9-dihexyl-9H-fluoren-2-yl)ethynyl)-9,9-dihexyl-9H-fluoren-2-yl)vinyl)-quinolizinium hexafluorophosphate (**2**).* To a refluxing acetonitrile solution (25 mL) of 2,8-dimethylquinolizinium hexafluorophosphate (**c**) (0.090 g; 0.30 mmol) and (7-((7-(diphenylamino)-9,9-dihexyl-9H-fluoren-2-yl)ethynyl)-9,9-dihexyl-9H-fluorene-2-carbaldehyde) (**j**) (0.800 g; 0.90 mmol) was), 4 mL of piperidine was added. After cooling the mixture to room temperature, a reddish precipitate came out of the solution and (150 mL) of hexane was added. The resulting precipitate was filtered and washed with ethanol. Purification was carried out by column chromatography using first CH_2Cl_2/MeOH (9:1) then CH_2Cl_2/acetonitrile (9:1). The pure compound was isolated as red solid. Yield: 35% (0.21 g). Mp: 138.5−139 °C. ^{1}H NMR (400 MHz, $CDCl_3$) δ: 8.72−8.70 (1 H, d, J = 7.3), 8.02−8.07 (1H, s), 7.75−7.81 (1H, d, J = 6.3), 7.52−7.72 (10H, m), 7.44−7.51 (1H, d, J = 7.9), 7.20−7.32 (5H, m), 7.11−7.20 (6H, m), 6.98−7.09 (3H, m), 2.56−2.68 (2H, q, J = 7.2), 2.03−2.23 (4H, m), 1.80−2.05 (6H, dddd, J = 28.7, 16.3, 11.5, 4.6), 1.05−1.30 (28H, dt, J = 25.1, 6.5), 0.85−1.02 (1H, m), 0.75−0.87 (13H, dt, J = 14.8, 7.1).). ^{13}C NMR (101 MHz, $CDCl_3$) 152.4, 152.1, 151.6, 150.7, 147.8, 147.6, 145.7, 143.2, 141.4, 140.1, 135.4, 133.9, 130.7, 129.1, 127.6, 126.0, 125.7, 123.9, 123.4, 122.87, 122.6, 122.5, 122.4, 121.6, 120.7, 120.5, 119.1, 119.0, 119.0, 91.5, 90.2, 55.4, 55.1, 46.2, 40.3, 31.6, 31.5, 29.7, 29.6, 23.7, 22.6, 22.5, 14.0. HR-MS (MALDI-DTL) calcd for $C_{141}H_{15}N_3$ $[M]^+$, 1894.2529; found for $C_{141}H_{15}N_3$ $[M]^+$, 1894.2472.

2.3. Linear Photophysical and Photochemical Measurements. The steady-state linear absorption, i.e., one-photon absorption (1PA), excitation, fluorescence, and excitation anisotropy spectra of **1** and **2**, along with their fluorescence lifetimes and photochemical stability, were investigated in air-saturated cyclohexane (CHX), toluene (TOL), tetrahydrofuran (THF), dichloromethane (DCM), and acetonitrile (ACN) at room temperature. 1PA spectra were measured with a UV−vis spectrophotometer (Agilent 8453) in 1-cm-path-length quartz cuvettes with molecular concentrations $C \approx (1-2) \times 10^{-5}$ M. The steady-state fluorescence, excitation, and excitation anisotropy spectra of **1** and **2** were obtained with a Quantamaster spectrofluorometer (PTI, Inc.) for dilute solutions ($C \approx 10^{-6}$ M), using 1-cm spectrofluorometric quartz cuvettes. All fluorescence and excitation spectra were corrected for the spectral responsivity of the PTI detection and excitation system. The measurements of the fluorescence quantum yield (Φ_{fl}) of **1** and **2** were performed by standard methodology,[29] relative to Coumarin 6 in ethanol as a reference ($\Phi_{fl} \approx 0.79$).[30] The fundamental excitation anisotropy spectra, $r(\lambda)$, were obtained in viscous silicon oil using an L-format configuration geometry.[29] The values of fluorescence lifetimes (τ_{fl}) were measured with a time-correlated single-photon-counting system PicoHarp 300 (time resolution of ∼80 ps), using 76 MHz femtosecond laser excitation (MIRA-900, Coherent Inc.), with linear polarization oriented by the magic angle. The photochemical decomposition quantum yields, Φ_{ph}, were determined for **1** and **2** in all employed solvents under UV lamp irradiation (LOCTITE 97034) with an excitation wavelength ($\lambda_{ex} \approx 436$ nm) and an average irradiance of 100 mW/cm^2. Corresponding values of Φ_{ph} were obtained by the absorption method previously described in detail.[31]

2.4. 2PA and Transient Absorption Measurements. The degenerate 2PA and transient absorption pump−probe measurements were performed using a femtosecond laser system (Coherent, Inc.) with two optical parametric amplifiers (OPA). All experimental aspects were previously described in detail.[32,33] Briefly, the output of a 76 MHz femtosecond Ti:sapphire laser (Mira 900-F, with a pulse duration (τ_p) of ∼180 fs, and exit wavelength of ∼800 nm) was regeneratively amplified by the Legend Elite (USP, Coherent, Inc.), providing a laser pulse train with $\tau_p \approx 100$ fs (fwhm), 1 kHz repetition rate, and pulse energy, $E_p \approx 4$ mJ. This laser output was divided into two equal parts that pumped two ultrafast OPAs (Opera Solo) with $E_p \leq 240$ μJ, $\tau_p \approx 100$ fs, and tuning range = 0.24−20 μ. The output from one of the OPA exits was used for degenerate 2PA cross-section measurements by the open-aperture Z-scan technique.[34] Transient absorption measurements were performed by a pump−probe method[33,35] with two laser beams from separate OPAs and an optical delay line (PI, Inc.). Possible photodecomposition and thermo-optical effects were avoided by employing a quartz flow cell with a path length of 1 mm.

2.5. Computational Details. To analyze the electronic properties of **1** and **2**, quantum-chemical calculations were performed with the Gaussian 09, Rev. A2 suite of programs.[36] Aliphatic side chains (C_6H_{13}) in **1** and **2**, which are not directly attached to the π-system, were replaced with methyl groups to save computer time. The resulting structures are denoted as **1a** and **2a**. We used DFT with the B3LYP functional[37] and the 6-31G* basis set[38] for geometry optimization. Electronically excited states were obtained at two levels of theory: TD-DFT (CAM-B3LYP[39]/6-31G*) and ZINDO/S. Solvent effects were simulated with the Polarizable Continuum Model (PCM), implemented in Gaussian 09, with dielectric constants corresponding to toluene, for both geometry optimization and the calculation of excitations. A positive net electric charge of +1 was applied to the entire structure. The electronic component of the 1PA and 2PA cross sections was calculated according to ref 40. The vertical excitations were calculated using the nonequilibrium solvation limit. Permanent and transition dipoles for the excited states were obtained in the dipole approximation[41] using TD-DFT with an unrelaxed density matrix.[42] The sum-over-state (SOS) formalism[43] with 12 singlet excited states was employed. The shape function for all spectral maxima was adopted to be Lorentzian with a half width at half-maximum (Γ) equal to 0.1

DOI: 10.1021/am508093p
ACS Appl. Mater. Interfaces 2015, 7, 2833−2846

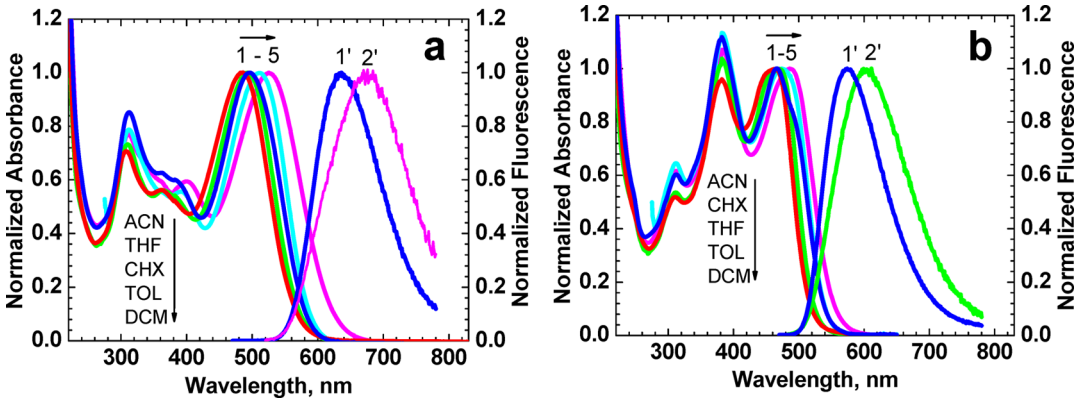

Figure 1. Normalized linear absorption (curves 1−5) and fluorescence (curves 1′ and 2′) spectra of (a) **1** and (b) **2** in different solvents. [Fluorescence spectra in CHX (1′) and TOL (2′).]

Table 1. Linear Photophysical and Photochemical Parameters of 1 in Solvents with Different Polarity

	1				
solvent	CHX	TOL	THF	DCM	ACN
polarity, Δf	0.000248	0.0135	0.209	0.217	0.305
absorption maxima, λ_{ab}^{max} (nm)	495 ± 1	510 ± 1	493 ± 1	525 ± 1	484 ± 1
fluorescence maxima, λ_{fl}^{max} (nm)	636 ± 1	673 ± 1			
Stokes shift (nm)	141 ± 2	163 ± 2			
Stokes shift (cm^{-1})	∼4480	∼4750			
maximum extinction coefficient, ε^{max} ($\times 10^{-3}$ M^{-1} cm^{-1})	42 ± 3	43 ± 3	48 ± 3	43 ± 3	49 ± 3
fluorescence quantum yield, Φ_{fl} (%)	46 ± 5	17 ± 5			
photodecomposition quantum yield, Φ_{ph} ($\times 10^4$)	0.5 ± 0.1	1 ± 0.2	0.06 ± 0.03	0.04 ± 0.02	2 ± 0.5
fluorescence lifetime, $\tau_{fl}{}^a$ (ns) (A_i)	3.3 ± 0.1	0.4 ± 0.1 (0.75) 1.9 ± 0.1 (0.25)			

[a]Obtained under an excitation wavelength of $\lambda_{ex} \approx 400$ nm.

Table 2. Linear Photophysical and Photochemical Parameters of 2 in Solvents with Different Polarity

	2				
solvent	CHX	TOL	THF	DCM	ACN
polarity, Δf	0.000248	0.0135	0.209	0.217	0.305
absorption maxima, λ_{ab}^{max} (nm)	466 ± 1	474 ± 1	469 ± 1	486 ± 1	463 ± 1
fluorescence maxima, λ_{fl}^{max} (nm)	574 ± 1	604 ± 1	∼502 (S_2)		
Stokes shift (nm)	108 ± 2	130 ± 2			
Stokes shift (cm^{-1})	∼4040	∼4540			
maximum extinction coefficient, ε^{max} ($\times 10^{-3}$ M^{-1} cm^{-1})	80 ± 3	74 ± 3	93 ± 3	83 ± 3	77 ± 3
fluorescence quantum yield, Φ_{fl} (%)	65 ± 5	26 ± 5	3 ± 0.5	<0.5	
photodecomposition quantum yield, Φ_{ph} ($\times 10^4$)	3 ± 1	2.7 ± 1	0.1 ± 0.03	0.035 ± 0.01	0.86 ± 0.3
fluorescence lifetime, $\tau_{fl}{}^a$ (ns)	2.8 ± 0.1	1.5 ± 0.1			

[a]Obtained under excitation wavelength of $\lambda_{ex} \approx 400$ nm.

eV. Natural transition orbital analysis of the TD-DFT excited state was done according to ref 44.

2.6. Bioimaging Methodology. *Determination of Bovine Serum Albumin (BSA) Binding Constants.* BSA solution (3 mL) was placed in a quartz cuvette with increasing concentration of quinolizinium added. The final concentration of BSA was maintained at 10 μM while the concentration of quinolizinium was varied over a range of 10−80 μM. Fluorescence emission spectra of BSA were recorded under the same conditions in the range of 300−400 nm, with excitation at 280 nm. The maximum emission intensity at 340 nm of each sample was recorded. The binding constant (K_a) was determined with the Scatchard equation,

$$\frac{r'}{c'} = n'K_a - r'K_a$$

where r' is the ratio of the concentration of bound ligand to total available binding sites, which can be calculated from the quenching of maximum emission intensity,[45,46] c' is the concentration of free drug, and n' is the number of binding sites for every BSA molecule. The value of K_a was obtained by plotting r'/c' against r'.

Cell Imaging. HeLa cells (ATCC) were seeded on poly-D-lysine-coated coverslips at a concentration of 5×10^4 cells/mL and incubated for 48 h. A stock solution of **1** in dimethyl sulfoxide (DMSO) was then diluted to 10 μM with MEM medium (Corning, Cellgro) and added to the cells. Cells were coincubated with a dilute solution of **1** together with Alexa Fluor 488 Conjugated Wheat Germ Agglutinin (AF-WGA, Life Technologies) for 15 min, then fixed with 4% formaldehyde. $NaBH_4$ was added twice at 1 mg/mL for 5 min to reduce autofluorescence. Coverslips were mounted on slides with ProLong Gold antifade reagent. Cell slides were imaged with a Leica SP5II microscope equipped with a Coherent Chameleon Vision S laser

DOI: 10.1021/am508093p
ACS Appl. Mater. Interfaces 2015, 7, 2833−2846

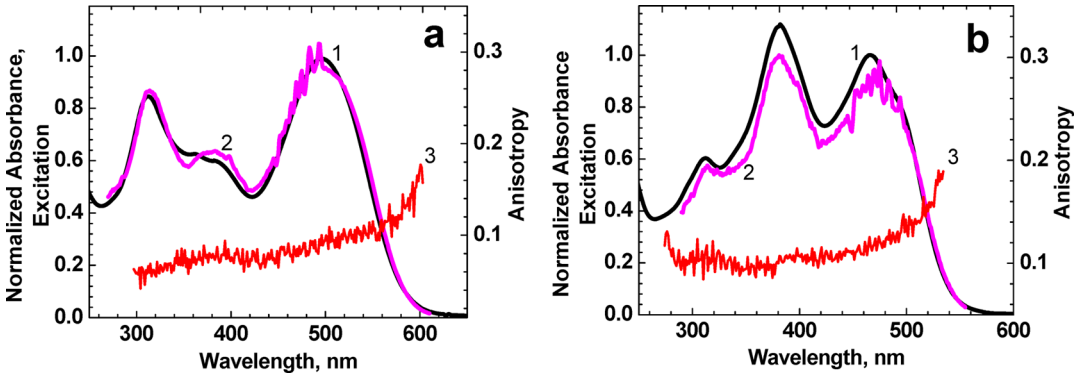

Figure 2. Normalized linear absorption (curve 1), excitation (curve 2), and excitation anisotropy (curve 3) spectra of (a) **1** and (b) **2** in CHX (curves 1 and 2) and in silicon oil (curve 3). Observed wavelength, λ_{obs} = 620 nm (panel a, curve 2) and 570 nm (panel b, curve 2).

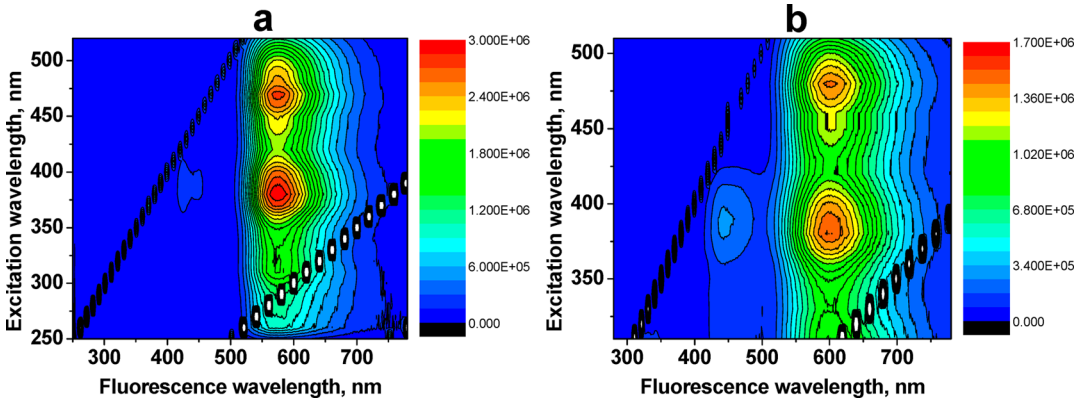

Figure 3. Three-dimensional (3D) fluorescence spectra of **2** in (a) CHX and (b) TOL.

source (prechirped compensated, 70 fs, 80 MHz). Probe **1** and AF-WGA were excited at 458 and 488 nm, respectively. Fluorescence was collected through a pinhole for confocal images in the range 700−800 nm for **1**, and 600−700 nm for AF-WGA. Images were scanned every 250 nm in the *z*-direction then processed with Amira software for 3D visualization.

3. RESULTS AND DISCUSSION

3.1. Linear Photophysical Properties and Photochemical Stability of 1 and 2. The electronic structures of the new quinolizinium fluorene-containing derivatives are D-π-A^+-π-D-type molecules with different π-conjugation lengths (recall Schemes 1 and 2), where D and A represent electron-donating and electron-accepting or deficient moieties, respectively. The steady-state 1PA spectra of **1** and **2** (Figure 1, curves 1−5) exhibit two well-defined absorption maxima (Figure 1a) and three well-defined absorption maxima (Figure 1b), respectively. The long-wavelength absorption bands with maxima at $\lambda_{ab}^{max} \approx$ 463−525 nm (see Tables 1 and 2) can be related to π−π^* electronic transitions concerned with the positively charged quinolizinium core. These long-wavelength bands exhibited a weak solvatochromic effect and complicated dependence on orientation polarizability Δf (this parameter defined by the expression $\Delta f = (\varepsilon - 1)/(2\varepsilon + 1) - (n^2 - 1)/(2n^2 + 1)$ can be a measure of solvent polarity, where ε and n are the dielectric constant and refraction index of the solvent, respectively).[29] The shortest long-wavelength absorption maximum was observed for the most polar solvent (ACN), and no monotonic dependence of λ_{ab}^{max} on Δf was detected. It is worth mentioning that the value of λ_{ab}^{max} decreases with the increase in π-conjugation length (i.e., from **1** to **2**), which reflects a weak intramolecular electronic interaction between fluorene and quinolizinium parts and an unusual hypsochromic effect via the extension of conjugation.[47] In this case, the fluorene moieties only play a role of quinolizinium end substituents with a certain electron-donating strength. The short-wavelength absorption bands at ∼310 nm and ∼380 nm, which presumably correspond to the fluorene fragments of **1** and **2**, were almost independent of solvent polarity and nicely correlated with the number of fluorene units.

The excitation anisotropy spectra of **1** and **2** (Figure 2, curves 3) revealed rather complicated nature of the main long-wavelength absorption bands, where a noticeable change in $r(\lambda)$ was observed, suggesting at least two electronic transitions in this spectral range.[29] The steady-state fluorescence spectra of **1** and **2** (Figures 1a and 1b, curves 1′ and 2′) also exhibited weak solvatochromic behavior and relatively large Stokes shifts of ∼4000−4800 cm^{-1}, even in low polarity solvents, which indicates sufficiently large changes in the optimized molecular geometry upon electronic excitation from $S_0 \rightarrow S_1$ (S_0 and S_1 are the ground and first excited electronic states, respectively).[48]

The corrected excitation spectra of **1** and **2** for the observed wavelength, λ_{obs}, in the spectral range of ∼550−750 nm (Figure 2, curve 2) nicely overlapped with the corresponding 1PA spectra (curve 1), which is evidence of only one fluorescence species in this spectral range. It is interesting to mention that three-dimensional (3D) fluorescence spectra of **2** (Figure 3) reveal an additional weak fluorescence band with a maximum at ∼425 nm. The total shape of this two-band fluorescence spectrum (including relative intensities at 425 and 574 nm)

DOI: 10.1021/am508093p
ACS Appl. Mater. Interfaces 2015, 7, 2833−2846

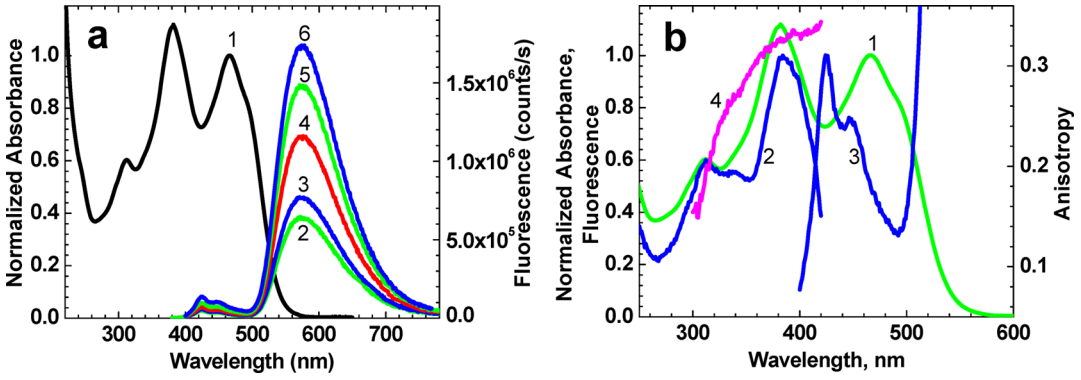

Figure 4. (a) Normalized linear absorption spectrum (curve 1) and fluorescence spectra (curves 2−6) of **2** in CHX: λ_{ex} = 330 nm (curve 2), 340 nm (curve 3), 360 nm (curve 4), 370 nm (curve 5), 390 nm (curve 6). (b) Normalized linear absorption (curve 1), excitation (curve 2) (λ_{obs} = 425 nm), fluorescence (curve 3) (λ_{ex} = 390 nm), and excitation anisotropy (curve 4) (λ_{obs} = 425 nm) spectra of **2** in CHX (curves 1−3) and silicon oil (curve 4).

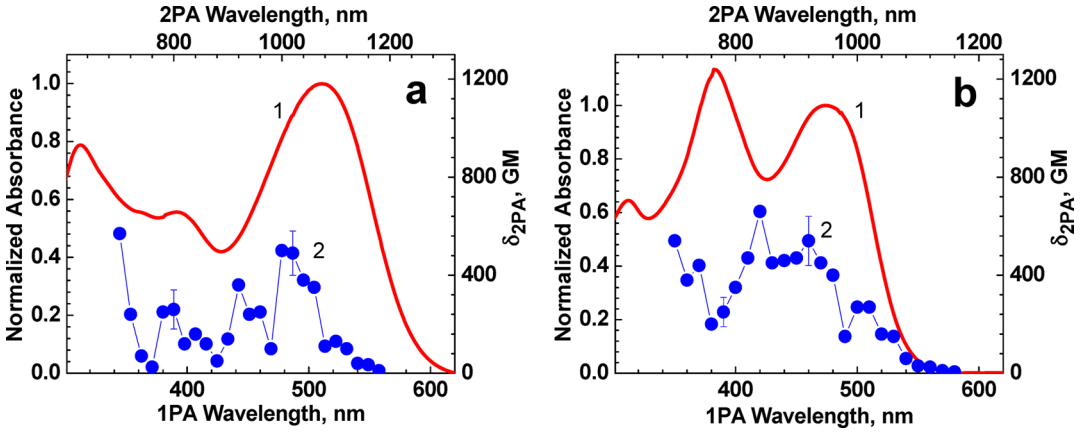

Figure 5. Normalized 1PA (curve 1) and degenerate 2PA (curve 2) spectra of (a) **1** and (b) **2** in TOL.

remained the same under the different excitation wavelengths in the spectral range of $\lambda_{ex} \leq 400$ nm (Figure 4a, curves 2−6). This means that the weak fluorescence band at 425 nm can be assigned to fluorescence emission from a higher excited electronic state S_n, which is evidence of Kasha's rule violation.[49] The shape and spectral position of the short-wavelength fluorescence band (Figure 4b, curve 3) and corresponding excitation spectrum (curve 2) are similar to the 1PA and fluorescence spectra for typical fluorene derivatives in nonpolar solvents[50−52] and can be attributed to the fluorene moieties of **2**. Relatively high values of the excitation anisotropy $r(\lambda) \approx 0.3$ (Figure 4b, curve 4) at the maximum of curve 2 also confirm this supposition.

Two different mechanisms can be considered to explain the nature of the weak short-wavelength fluorescence contour with $\lambda_{fl}^{max} \approx 425$ nm observed under excitation at $\lambda_{ex} \leq 400$ nm. The first is concerned with only one type of solvated molecule of **2** with a high excited electronic level S_n exhibiting a relatively long lifetime, assumingly ∼50−100 ps, from which short wavelength fluorescence emission occurs. The second mechanism can be related to a small number of highly fluorescent and specifically solvated molecules of **2** formed in the excited state S_n. In this case, most of the molecules in the solution are not specifically solvated and exhibit only one long wavelength fluorescence emission band related to the first excited state S_1 in accordance with Kasha's rule. The formation of specifically solvated chromophores can be a result of symmetry-breaking effects in the excited state of **2**, as was reported previously for some fluorene derivatives.[53] The fluorescence quantum yields, Φ_{fl}, were obtained under excitation at the maximum of the main long wavelength absorption band and exhibited a strong dependence on solvent polarity (see Tables 1 and 2), which confirms an important role of solvation processes on the electronic structures of **1** and **2**. Fluorescence lifetimes were in the range of 0.5−3.3 ns and the observed emission decay curves corresponded to a single exponential process, except for **1** in TOL, where a relatively weak long-decay-time component was observed (Tables 1 and 2).

Photochemical stability of **1** and **2** was investigated under continuous-wave UV lamp irradiation, and the corresponding values of the photodecomposition quantum yields Φ_{ph} were in therange of $\sim 3 \times 10^{-4}$−3×10^{-6} (see Tables 1 and 2). Simple estimations of photodecomposition rate constants were performed taking into account a strong dependence of fluorescence quantum yields Φ_{fl} on solvent polarity. A complicated dependence on solvent type was observed, and the lowest rate constant value $\sim 1.5 \times 10^4$ s^{-1} was obtained for **1** in nonpolar CHX. It should be mentioned that the level of photochemical stability exhibited by **1** and **2** is not as high as that reported for some fluorene labels,[54−56] but is acceptable for practical bioimaging.

3.2. 2PA Properties of 1 and 2. Degenerate 2PA spectra of symmetrical fluorene-containing quinolizinium structures **1** and **2** were obtained over a broad spectral range by an open-aperture Z-scan technique[34] and are shown in Figure 5. In contrast to the previously reported quinolizinium derivative V-

DOI: 10.1021/am508093p
ACS Appl. Mater. Interfaces 2015, 7, 2833−2846

DMA2,[11] fluorene-containing **1** and **2** exhibited a entirely different 2PA spectral contour. Fluorenyl quinoliziniums **1** and **2** are not centrosymmetric and exhibit relatively large 2PA cross sections, δ_{2PA}, in the spectral range of the main long-wavelength linear absorption bands, at least three well-defined 2PA maxima were observed for the simpler compound **1** (Figure 5a, curve 2), and the most intense, with $\delta_{2PA} \approx 500$ GM, is sufficiently close to the main 1PA contour. It should be mentioned that the obtained excitation anisotropy data and weak solvatochromic effects in the steady-state fluorescence spectra (Figure 1) indicate a small contribution of the dipolar term (i.e., of the product $\sim|\Delta\boldsymbol{\mu}_{01}|^2|\boldsymbol{\mu}_{01}|^2$, where $\Delta\boldsymbol{\mu}_{01}$ is the change in the permanent dipole moment under electronic excitation $S_0 \rightarrow S_1$, and $\boldsymbol{\mu}_{01}$ is the transition dipole moment for the $S_0 \rightarrow S_1$ transition)[43] to the values of δ_{2PA}, and a dominant role of two-photon terms for $S_0 \rightarrow S_n$ ($n > 1$) two-photon transitions. In the case of the more-complicated compound **2**, a broad 2PA spectrum with $\delta_{2PA} \approx 400-600$ GM was observed, and the same nature of two-photon transitions can be assumed. Taking into account the relatively high fluorescence quantum yield of **2** (~0.65), large 2PA cross sections and nice overlap of its 2PA spectrum with the tuning range of commercial Ti:sapphire lasers, its high potential for fluorescence microscopy applications is anticipated.

3.3. Transient Absorption Spectroscopy of 1 and 2. Fast relaxation processes in the electronically excited states of **1** and **2** were investigated in TOL solution at room temperature by the well-developed femtosecond pump−probe transient absorption method,[33,35] using a 1-mm-path-length quartz flow cell. Transient absorption curves, $\Delta D = f(\tau_D)$ (where ΔD and τ_D are the induced optical density and time delay between pump and probe pulses, respectively) were obtained for two-pump wavelengths (λ_{pm} = 400 nm ($S_0 \rightarrow S_n$ excitation) and λ_{pm} = 500 nm ($S_0 \rightarrow S_1$ excitation)) and for different probe wavelengths (λ_{pr}), over the broad spectral range of 500−800 nm (Figure 6).

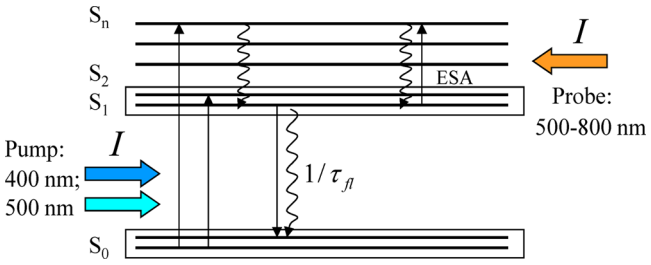

Figure 6. Simplified schematic diagram of the electronic structure of the investigated compounds with fast dynamic processes and corresponding experimental pump−probe conditions (see text for details).

The most characteristic dependencies, $\Delta D = f(\tau_D)$, for some λ_{pr} values are presented in Figure 7. Note that dependencies in Figures 7a′−h′ are not the extended parts of those in Figures 7a−h but were obtained independently with a different time step, which is evidence of the high reproducibility of these experimental results. As follows from Figures 7a and 7a′, as well as Figures 7e and 7e′, negative values of ΔD that appeared within 0.3−0.5 ps for λ_{pr} = 500 nm (i.e., in the main 1PA bands of **1** and **2**) can be attributed to the depopulation of the ground state S_0. An additional longer relaxation process with a characteristic time of ~1.5−2 ps was also observed in this spectral range, as evidence of some role of excited-state absorption (ESA), along with Franck−Condon and/or solvate relaxation dynamics.[29,57,58] ESA processes (i.e., $\Delta D > 0$) were more obviously revealed at the long-wavelength edge of 1PA band for λ_{pr} = 560 nm (Figure 7b for **1**) and λ_{pr} = 540 nm (Figure 7f for **2**). The sharp peak in the ultrafast dynamics of **2** at λ_{pr} = 540 nm (Figure 7f′) can be explained by the short-lived ESA from a higher excited electronic state, S_n, with a following fast relaxation to the S_1 and decreasing relative influence of the ground-state depopulation. In the fluorescence spectral range (λ_{pr} > 600 nm), only ESA processes were observed (Figure 7, two right columns of plots), except for **1** at λ_{pr} = 740 nm (Figure 7d), where a weak stimulated emission phenomenon ($\Delta D < 0$) occurred. The temporal shapes of the curves $\Delta D = f(\tau_D)$ obtained under different pumping conditions (λ_{pm} = 500 nm ($S_0 \rightarrow S_1$) and λ_{pm} = 400 nm ($S_0 \rightarrow S_n$) excitations) were almost the same for all probe wavelengths. The largest temporal delay of ~200 fs was observed for λ_{pr} = 680 nm (see Figure 8). This means that most of the excited states of **1** and **2** exhibited a fast vibronic relaxation $S_n \rightarrow S_1$ in the subpicosecond time scale and no violation of Kasha's rule should be observed. Hence, the second mechanism for the explanation of a weak fluorescence emission observed from the S_n state (see section 3.1) seems to be more probable.

Transient pump−probe absorption spectra of **1** and **2**, reconstructed from the experimentally obtained dependences $\Delta D = f(\tau_D)$ in the broad spectral range of λ_{pr}, are presented in Figure 9. According to this data, no appreciable temporal spectral shift in the ESA spectrum was observed for **2** (see Figure 9b). In contrast, an obvious hypsochromic spectral shift was observed in the ESA band of **1** (Figure 9a). It is worth mentioning that an almost constant value of ΔD for **1** at ~660 nm is not a real isosbestic point and observed only for presented particular delays. Presumably, this difference in ESA properties of the investigated molecules reflects a higher density of vibronic states in the electronic structure of the more-complicated compound **2**. It should be mentioned that, despite the observed stimulated emission in the fluorescence spectral range (Figure 9a, curve 3), no superfluorescence and lasing phenomena were observed for **1** under femtosecond pumping.

3.4. Quantum Chemical Modeling of the Electronic Properties of 1 and 2. The optimized structure of **2a** is shown in Figure 10. The DFT optimization essentially made the geometry close to planar, except for the methyl and phenyl groups. The latter are twisted off the plane by 71° ± 2° for **1a** and by 67° ± 2° for **2a**. The symmetry is close to the C_{2v} point group, so this was used to interpret results. 1PA spectra simulated at the TD-B3LYP/6-31+G* and ZINDO/S levels of theory are shown in Figure 11, in comparison with experimental data. ZINDO/S simulations satisfactorily reproduce the entire 1PA spectra, although the first (long-wavelength) maximum is somewhat red-shifted, with respect to the experimentally observed peak. If one imagines that it shifted to the experimental wavelength, then, together with the second (small) maximum, they would produce a broadened first peak, similar to that which takes place on the experimental curves. The second high maximum for **2**/**2a**, at ~400 nm, is well-reproduced by ZINDO/S calculations and composed of two quasi-degenerate excited states: S_3 and S_4. Obviously, oscillator strengths for the S_3 and S_4 states in **1**/**1a** are lower than in **2**/**2a**, and are better resolved in energy.

The third experimental peak, at ~310 nm for both **1** and **2**, is again formed by two quasi-degenerate excited states, according

DOI: 10.1021/am508093p
ACS Appl. Mater. Interfaces 2015, 7, 2833−2846

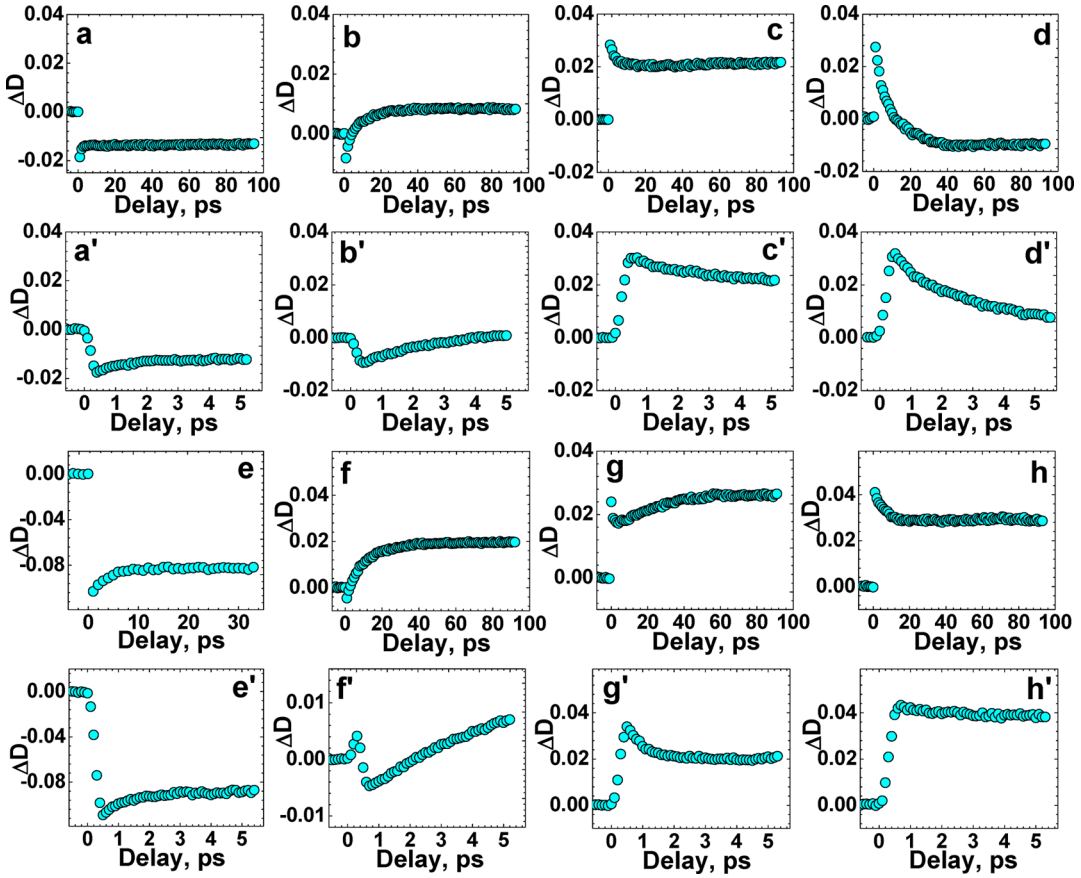

Figure 7. Transient absorption dependences, $\Delta D = f(\tau_D)$, for **1** (panels (a)−(d); (a′)−(d′)) and **2** (panels (e)−(h); (e′)−(h′)) in TOL under pumping at λ_{pm} = 400 nm: λ_{pr} = 500 nm (a, a′), 560 (b, b′), 660 nm (c, c′), 740 nm (d, d′), 500 nm (e, e′), 540 nm (f, f′), 600 nm (g, g′), and 700 nm (h, h′).

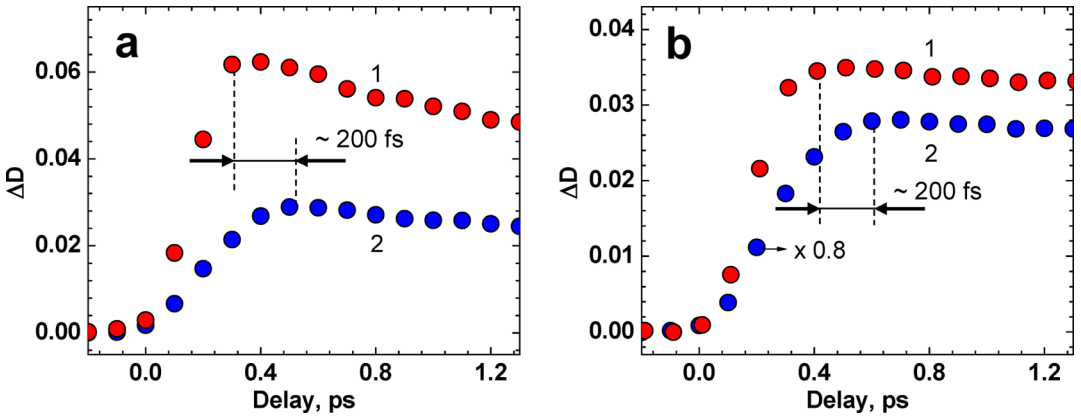

Figure 8. Transient absorption dependences, $\Delta D = f(\tau_D)$, for (a) **1** and (b) **2** in TOL under pumping at λ_{pm} = 500 nm (curve 1) and 400 nm (curve 2): λ_{pr} = 680 nm.

to the ZINDO/S calculations. The TD-CAM-B3LYP calculations nicely reproduce the position of the first peak represented by the S_1 and S_2 states (see Table 3). However, the shorter-wavelength region is somewhat blue-shifted. The TD-CAM-B3LYP level of theory predicts negligible oscillator strengths for the S_3 and S_4 states in **1a**. Their role involves the S_5 and S_7 states. The 2PA cross section is considerably overestimated at the wavelength corresponding to excitation of the S_2 state for both **1a** and **2a** (see Table 3). This is likely because the transition dipole $\boldsymbol{\mu}_{12}$ is overestimated. However, the same transition dipole contributes to 2PA to S_1. Thus, by fitting only a single parameter (e.g., $\boldsymbol{\mu}_{12}$), it is impossible to correct the entire spectrum. To match the 2PA spectra at the wavelength range of the first two excited states, it is necessary to fit one more parameter (e.g., $\boldsymbol{\mu}_{11}$). We found that the combinations $\Delta\boldsymbol{\mu}_{01}$ = 14 D, $\boldsymbol{\mu}_{12}$ = 7 D for **1a**, and $\Delta\boldsymbol{\mu}_{01}$ = 9.7 D, $\boldsymbol{\mu}_{12}$ = 9.7 D for **2a** match the experimental 2PA cross sections for the first two excited states. Apparently, this is an artifact of the unrelaxed density matrix approach used in our calculation of the transition dipoles.

The natural transition orbitals (NTOs) for the states listed in Table 3 are shown in Table S1 in the Supporting Information.

DOI: 10.1021/am508093p
ACS Appl. Mater. Interfaces 2015, 7, 2833−2846

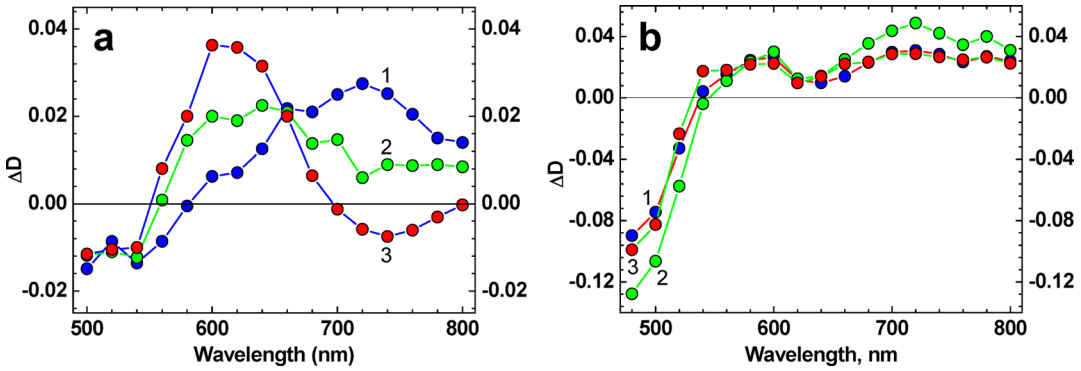

Figure 9. Transient pump–probe absorption spectra of (a) **1** and (b) **2** in TOL at λ_{pm} = 400 nm [in panel (a), τ_D = 0.3 ps (curve 1), 5 ps (curve 2), and 30 ps (curve 3); in panel (b), τ_D = 0.3 ps (curve 1), 0.6 ps (curve 2), and 30 ps (curve 3)].

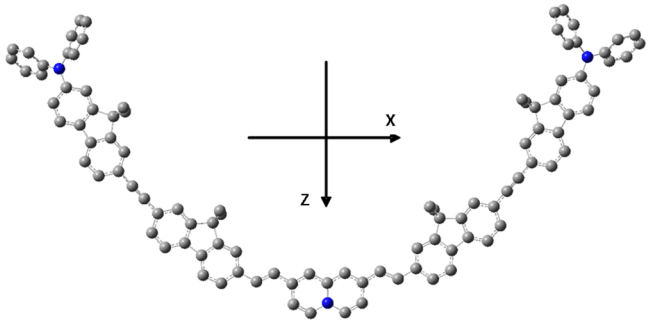

Figure 10. Optimized structure of **2a** at the DFT(B3LYP)/6-31G*/PCM(TOL) level of theory. Cartesian axes are also shown.

Some are close to conventional orbitals. Therefore, all of the states, except of S_7 in **1a**, are transitions to one particular orbital, which is approximately equal to the LUMO and belongs to the b_2 representation of the C_{2v} group. The "hole" NTOs belong to the a_2 or b_2 representations consecutively, producing the states of B_1 or A_1 representations, respectively. The X-component of the dipoles, transformed according to the B_1 representation, has the largest values. The second-largest component of the dipoles is Z, which is symmetric in C_{2v}. Accordingly, the maximal 1PA probability appears for the states belonging to B_1, and the second large probability belongs to the A_1 representation. Conversely, the largest 2PA cross sections were observed for A_1 states, and somewhat lower 2PA cross sections were observed for B_1 states.

3.5. Fluorescence Bioimaging. It was reported that quinolizinium derivatives can bind with biomacromolecules such DNA and proteins, exhibiting a fluorescence turn-on effect, because of a restricted conformation flexibility.[59,60] Similar effects were observed with quinoliziniums **1** and **2**. Although not fluorescent in polar media, the probes exhibited noticeable fluorescence turn-on behavior upon binding BSA, resulting in more than 4-fold fluorescence enhancement (see Figure S1 in the Supporting Information). The fluorescence stopped increasing after the dye-to-BSA ratio reached ~0.4–0.5. When plotted for quenching of BSA fluorescence with Stern–Volmer curves, both probes gave a nonlinear relation (data not shown). These results indicate that the binding of probes and BSA is not in a 1:1 ratio. It could be assumed, according to the binding results, that one quinolizinium molecule may bind with more than one BSA molecule. A similar BSA quenching pattern was reported with other quinolizinium structures;[16] however, a detailed binding mechanism has not been elucidated. Further studies are necessary to determine the binding sites and binding pattern of these new quinoliziniums. Since Stern–Volmer plots are applied for linear stoichiometric binding,[16,61,62] a different method was employed to determine the BSA binding constant: Scatchard plot analysis.[45,46] Both probes showed strong affinity to BSA and sufficient fluorescence increase upon binding (Figure 12). This solves the problem of low fluorescence in polar solvents and supported their further application in

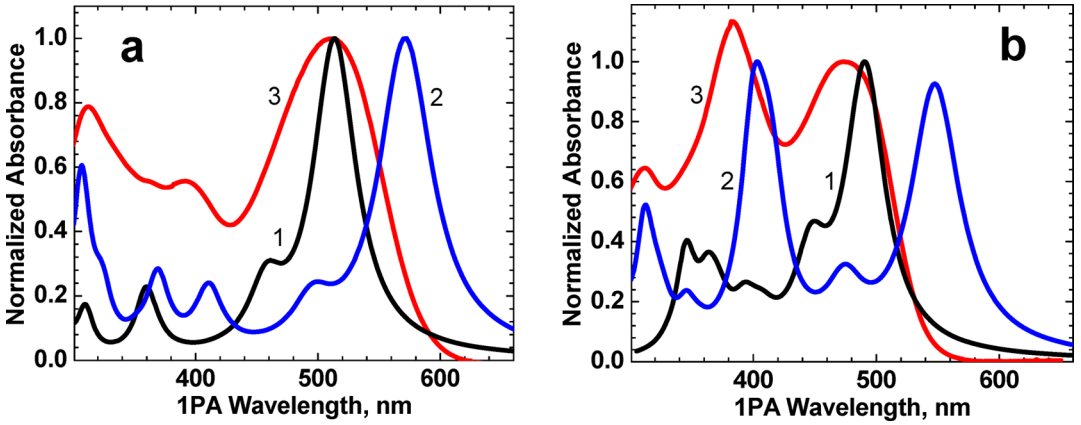

Figure 11. Calculated 1PA spectra (1, 2) of (a) **1a** and (b) **2a**, in comparison with experimental 1PA spectra (curve 3) of **1** and **2** in TOL. Curves 1 and 2 are obtained at the TD-CAM-B3LYP/6-31G* and ZINDO/S levels of theory, respectively, using PCM (TOL).

DOI: 10.1021/am508093p
ACS Appl. Mater. Interfaces 2015, 7, 2833–2846

Table 3. Permanent μ_{ii} and Transition Dipole Moments μ_{ij} (in Debye) Obtained at the TD-CAM-B3LYP/6-31G* Level of Theory for the Ground (S_0) and Excited States (S_j) That Essentially Contribute to the 2PA of the First Two Excited States (S_1 and S_2)[a]

	0		1		2			δ_{2PA} (GM)	
state #	X	Z	X	Z	X	Z	En (eV)	**1a** (theor.)	**1** (exp.)
1	**−18.2**	0.00	−0.02	**−5.42**	**12.7**	0.00	2.41	129	500
2	−0.01	**7.49**	**12.7**	0.00	0.02	**−7.37**	2.71	1310	360
5	**6.73**	−0.01	−0.01	−4.45	**12.0**	0.00	3.45		
7	−0.01	**5.06**	**−5.18**	0.00	−0.02	2.97	4.00		
	0		1		2			δ_{2PA} (GM)	
state #	X	Z	X	Z	X	Z	En (eV)	**2a** (theor.)	**2** (exp.)
1	**−19.4**	−0.02	−0.03	**−6.90**	**−14.8**	−0.01	2.52	196	270
2	0.02	**−10.2**	**−14.8**	−0.01	0.03	**−15.2**	2.77	1480	540
3	**5.05**	0.01	−0.03	**−8.61**	**−21.0**	0.00	3.04		
4	−0.01	**6.16**	**−5.80**	0.00	0.02	**−12.6**	3.15		

[a]Columns X and Z stand for projections of the dipoles defined in Figure 10. The ground-state dipole moment has been subtracted from the permanent dipoles. The other columns contain transition energies En = E_{0j} in eV, obtained at the same level of theory, and the 2PA cross-section δ_{2PA} in GM for the first two excited states were obtained theoretically (theor.) and experimentally (exp.). The top half of the table corresponds to **1a**/**1**, and the bottom half corresponds to **2a**/**2**.

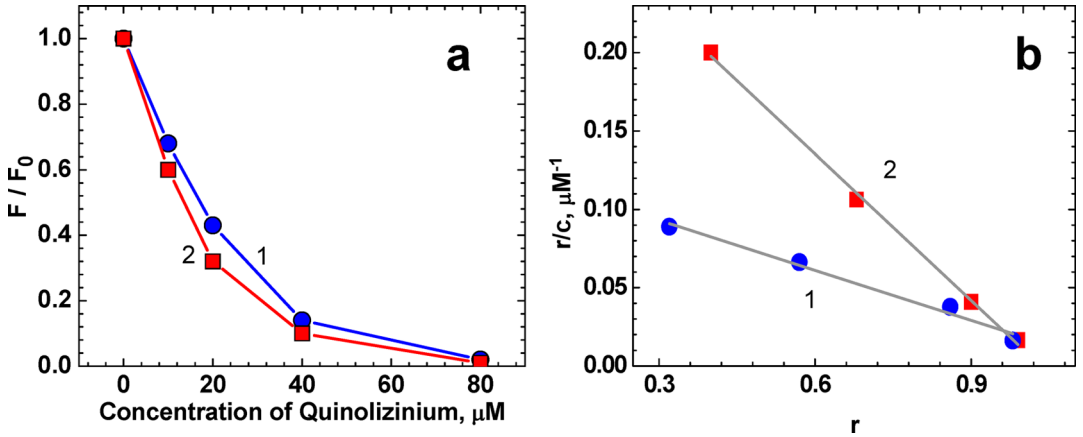

Figure 12. (a) Quenching curves of BSA (λ_{ex} = 280 nm, λ_{em} = 340 nm) by binding with quinolizinium **1** (curve 1) and **2** (curve 2) at different ratios. F and F_0 are the intensities of BSA fluorescence emission with and without binding, respectively. (b) Scatchard plots for BSA binding constants of quinoliziniums. K_a for **1** (curve 1) and **2** (curve 2) are 1.1 × 10^5 M^{-1} and 3.1 × 10^5 M^{-1}, respectively.

bioimaging. However, poor solubility in DMSO prohibited further study of **2** in cell imaging.

Cells exhibited bright fluorescence at the wavelength range corresponding to emission of **1** (Figure 13). Three-dimensional (3D) visualization suggested that the observed fluorescence of **1** was localized on cell membranes. Fluorescently labeled wheat germ agglutinin (WGA) is used to detect glycoconjugates on cell membranes by selectively binding to *N*-acetylglucosamine and *N*-acetylneuraminic acid residues (see Figure 13C).[63] Hence, a co-incubation experiment was performed to assess if probe **1** was localizing on cell membranes. Overlay of two dyes (Alexa Fluor 488-WGA and **1**, Figure 13D) indicates that **1** may localize on the cell membrane but bind with different membrane components than WGA. Considering the low emission efficiency of **1** as a free dye in DMSO-H_2O mixture (Figure S1 in the Supporting Information), bright fluorescence images of **1** (Figure 13B) support enhancement of its fluorescence upon binding with cell membrane proteins. Co-incubation of **1** with anti-α-tubulin antibody, phalloidin, or antivinculin shows different degrees of overlap. Among the three proteins examined, the distribution of **1** appeared to be more associated with vinculins (Figure S2 in the Supporting Information).

4. CONCLUSIONS

The linear photophysical and photochemical properties, along with 2PA and femtosecond transient absorption spectroscopy, of new fluorene-containing symmetrical quinolizinium derivatives **1** and **2** were investigated. Linear absorption spectra exhibited a weak and rather complicated dependence on solvent polarity. The steady-state fluorescence, excitation, and excitation anisotropy spectra revealed the nature of the dual-band fluorescence emission of **2** and the complex electronic structure of the main long-wavelength absorption band. The short-wavelength fluorescence band of **2**, with a maximum at ∼425 nm, was attributed to emission from a higher excited electronic state S_n, which is evidence of Kasha's rule violation for this molecular type. Symmetrical cations **1** and **2** exhibited different contours of degenerate 2PA spectra with maximal cross sections δ_{2PA} ≈ 400−600 GM and an extended full width at half-maximum of the more-complex compound **2**. Ultrafast dynamic processes in the ground and excited electronic states of **1** and **2** revealed two different types of relaxations with

DOI: 10.1021/am508093p
ACS Appl. Mater. Interfaces 2015, 7, 2833−2846

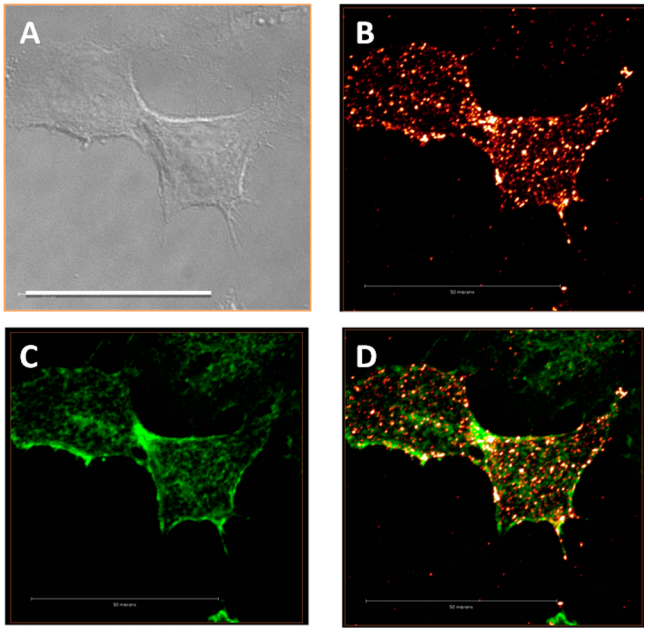

Figure 13. (A) DIC and (B, C) fluorescent images of HeLa cells co-incubated with **1** (panel (B)) and Alexa Fluor 488-WGA (panel (C)). Fluorescent images were acquired by scanning every 250 nm in the *z*-direction and then processed with Amira software. (D) Overlay image of panels (B) and (C). [Scale bar = 50 μm.]

characteristic times of 0.3−0.5 ps and 1.5−2 ps, which can be explained by fast vibronic $S_n \rightarrow S_1$ transitions and solvate reorganization phenomena. The electronic, linear, and nonlinear optical properties of **1** and **2** were modeled with quantum-chemical calculations. The 1PA spectra obtained in both the TD-CAM-B3LYP and ZINDO/S approaches were in good agreement with the experimental data. Theoretically predicted 2PA cross sections for the wavelength corresponding to the second excited states were overestimated. Apparently, this is because the transition dipole between the first and second excited states was overestimated by our calculations.

Although not fluorescent in polar media, the dyes exhibited fluorescence turn-on behavior upon binding BSA, exhibiting over 4-fold fluorescence enhancement. Advantageous linear photophysical and photochemical properties, good 2PA cross sections, and nice overlap of the 2PA spectra with the tuning range of commercial Ti:sapphire lasers, suggested the potential of new quinolizinium derivatives for laser scanning fluorescence microscopy applications. High BSA binding and bright membrane-localized fluorescence images of HeLa cells confirmed this and will be the subject of expanded studies.

■ ASSOCIATED CONTENT

Supporting Information

Fluorescence emission of **1** and **2** with BSA and colocalization studies of **1** in HeLa cells. This material is available free of charge via the Internet at http://pubs.acs.org.

■ AUTHOR INFORMATION

Corresponding Author

*E-mail: belfield@njit.edu.

Notes

The authors declare no competing financial interest.

■ ACKNOWLEDGMENTS

We wish to acknowledge the National Science Foundation (Nos. CBET-1517273, ECCS-0925712, CHE-0840431, and CHE-0832622), the U.S. National Academy of Sciences (No. PGA-P210877), the National Academy of Sciences of Ukraine (Grant Nos. 1.4.1.B/153 and VC/157), and the People Programme (Marie Curie Actions) of the European Union's Seventh Framework Programme FP7/2007-2013/ under REA grant agreement n°607721. Calculations were performed using the HPCC facilities of the I^{2}Lab (Interdisciplinary Information Science and Technology Laboratory) at the University of Central Florida.

■ REFERENCES

(1) Sato, K.; Okazaki, S.; Yamagishi, T.; Arai, S. The Synthesis of Azoniadithia[6]helicenes. *J. Heterocyclic Chem.* **2004**, *41*, 443−447.
(2) Osbond, J. M. Chemical Constitution and Amoebicidal Activity. VI. A New Synthesis of 2-Ketones and 2-Alcohols Derived from 3-Alkyl-1,3,4,6,7,11b Hexahydro-9,10-Dimethoxy-2h-Benzo-[a]-quinolizines. *J. Chem. Soc.* **1961**, 4711−4718.
(3) Tian, M.; Ihmels, H. Selective Colorimetric Detection of Hg^{2+} and Mg^{2+} with Crown Ether Substituted *N*-Aryl-9-aminobenzo[b]-quinolizinium Derivatives. *Eur. J. Org. Chem.* **2011**, 4145−4153.
(4) Tian, M.; Ihmels, H.; Ye, S. Fluorimetric Detection of Mg^{2+} and DNA with 9-(Alkoxyphenyl)benzo[b]quinolizinium Derivatives. *Org. Biomol. Chem.* **2012**, *10*, 3010−3018.
(5) Ihmels, H.; Salbach, A. Efficient Photoinduced DNA Damage by Coralyne. *Photochem. Photobiol.* **2006**, *82*, 1572−1576.
(6) Ihmels, H.; Faulhaber, K.; Vedaldi, D.; Dall'Acqua, F.; Viola, G. Intercalation of Organic Dye Molecules into Double-Stranded DNA. Part 2: The Annelated Quinolizinium Ion as a Structural Motif in DNA Intercalators. *Photochem. Photobiol.* **2005**, *81*, 1107−1115.
(7) Viola, G.; Bressanini, M.; Gabellini, N.; Vedaldi, D.; Dall'Acqua, F.; Ihmels, H. Naphthoquinolizinium Derivatives as a Novel Platform for DNA-Binding and DNA-Photodamaging Chromophores. *Photochem. Photobiol. Sci.* **2002**, *1*, 882−889.
(8) Zhuo, G.; Wang, X.; Wang, D.; Wang, C.; Zhao, X.; Shao, Z.; Jiang, M. Two-Photon Induced Optical-Power Limiting and Upconverted Superradiance Properties of a New Organic Dye HEASPI. *Opt. Laser Technol.* **2001**, *33*, 209−212.
(9) Bellier, Q.; Makarov, N. S.; Bouit, P.-A.; Rigaut, S.; Kamada, K.; Feneyrou, P.; Berginc, G.; Maury, O.; Perry, J. W.; Andraud, C. Excited State Absorption: A Key Phenomenon for the Improvement of Biphotonic Based Optical Limiting at Telecommunication Wavelengths. *Phys. Chem. Chem. Phys.* **2012**, *14*, 15299−15307.
(10) Kopylova, T. N.; Svetlichnyi, V. A.; Mayer, G. V.; Reznichenko, A. V.; Podgaetskii, V. M.; Ponomareva, O. V.; Samsonova, L. G.; Filinov, D. N.; Pomogaev, V. A.; Tel'minov, E. N.; Lapin, I. N.; Svetlichnaya, N. N.; Sinchenko, E. I. Limitation of High-Power Optical Radiation by Organic Molecules: I. Substituted Pyranes and Cyanine Dyes. *Quantum Electron.* **2003**, *33*, 967−974.
(11) Macoas, E.; Marcelo, G.; Pinto, S.; Caneque, T.; Cuadro, A. M.; Vaquero, J. J.; Martinho, J. M. G. A V-Shaped Cationic Dye for Nonlinear Optical Bioimaging. *Chem. Commun.* **2011**, *47*, 7374−7376.
(12) Zhou, S.; Zhang, Q.; Tian, X.; Hu, G.; Hao, F.; Wu, J.; Tian, Y. Synthesis, Crystal Structure, Optical Properties, DNA-Binding and Cell Imaging of an Organic Chromophore. *Dyes Pigm.* **2011**, *92*, 689−695.
(13) Nag, O. K.; Nayak, R. R.; Lim, C. S.; Kim, I. H.; Kyhm, K.; Cho, B. R.; Woo, H. Y. Two-Photon Absorption Properties of Cationic 1,4-Bis(styryl)benzene Derivative and Its Inclusion Complexes with Cyclodextrins. *J. Phys. Chem. B* **2010**, *114*, 9684−9690.
(14) Ho, H.-A.; Najari, A.; Leclerc, M. Optical Detection of DNA and Proteins with Cationic Polythiophenes. *Acc. Chem. Res.* **2008**, *41*, 168−178.

DOI: 10.1021/am508093p
ACS Appl. Mater. Interfaces 2015, 7, 2833−2846

(15) Granzhan, A.; Ihmels, H. *N*-Aryl-9-amino-substituted Acridizinium Derivatives as Fluorescent "Light-up" Probes for DNA and Protein Detection. *Org. Lett.* **2005**, *73*, 5119−5122.
(16) Faulhaber, K.; Granzhan, A.; Ihmels, H.; Otto, D.; Thomas, L.; Wells, S. Studies of the Fluorescence Light-up Effect of Amino-Substituted Benzo[b]quinolizinium Derivatives in the Presence of Biomacromolecules. *Photochem. Photobiol. Sci.* **2011**, *10*, 1535−1545.
(17) Tokar, V. P.; Losytskyy, M. Y.; Ohulchanskyy, T. Y.; Kryvorotenko, D. V.; Kovalska, V. B.; Balanda, A. O.; Dmytruk, I. M.; Prokopets, V. M.; Yarmoluk, S. M.; Yashchuk, V. M. Styryl Dyes as Two-Photon Excited Fluorescent Probes for DNA Detection and Two-Photon Laser Scanning Fluorescence Microscopy of Living Cells. *J. Fluoresc.* **2010**, *20*, 865−872.
(18) Yashchuk, V. M.; Yu. Kudrya, V. Y.; Losytskyy, M. Y.; Tokar, V. P.; Yarmoluk, S. M.; Dmytruk, I. M.; Prokopets, V. M.; Kovalska, V. B.; Balanda, A. O.; Kryvorotenko, D. V.; Ogul'chansky, T. Y. The Optical Biomedical Sensors for the DNA Detection and Imaging Based on Two-Photon Excited Luminescent Styryl Dyes. Phototoxic Influence on the DNA. *Proc. SPIE* **2007**, *6796*, 67960M/1−67960M/14.
(19) Wang, J.; Burdzinski, G.; Zhu, Z.; Platz, M. S.; Carra, C.; Bally, T. Ultrafast Spectroscopic and Matrix Isolation Studies of *p*-Biphenylyl, *o*-Biphenylyl, and 1-Naphthylnitrenium Cations. *J. Am. Chem. Soc.* **2007**, *129*, 8380−8388.
(20) Malval, J.-P.; Chaumeil, H.; Rettig, W.; Kharlanov, V.; Diemer, V.; Ay, E.; Morlet-Savary, F.; Poizat, O. Excited-State Dynamics of Phenol−Pyridinium Biaryl. *Phys. Chem. Chem. Phys.* **2012**, *14*, 562−574.
(21) Furuta, K.; Fuyuki, M.; Wada, A. Multiphoton Reaction of DTTCI Observed by Femtosecond Pump-Probe and Two-Pulse Correlation Measurements. *Chem. Phys.* **2013**, *418*, 42−46.
(22) Ramírez, M. A.; Cuadro, A. M.; Alvarez-Builla, J.; Castaño, O.; Andrés, J. L.; Mendicuti, F.; Clays, K.; Asselberghs, I.; Vaquero, J. J. Donor-(p-bridge)-Azinium as D-p-A^+ One-Dimensional and D-p-A^+-p-D Multidimensional V-Shaped Chromophores. *Org. Biomol. Chem.* **2012**, *10*, 1659−1669.
(23) Faulhaber, K.; Granzhan, A.; Ihmels, H.; Viola, G. Detection of Biomacromolecules with Fluorescent Light-up Probes. *Pure Appl. Chem.* **2006**, *78*, 2325−2331.
(24) Barbafina, A.; Amelia, M.; Latterini, L.; Aloisi, G. G.; Elisei, F. Photophysical Properties of Quinolizinium Salts and Their Interactions with DNA in Aqueous Solution. *J. Phys. Chem. A* **2009**, *113*, 14514−14520.
(25) Thompson, M. A.; Zerner, M. C. A Theoretical Examination of the Electronic Structure and Spectroscopy of the Photosynthetic Reaction Center from *Rhodopseudomonas Viridis*. *J. Am. Chem. Soc.* **1991**, *113*, 8210−8215.
(26) Zerner, M. C., Semiempirical Molecular Orbital Methods. In *Reviews of Computational Chemistry*, Lipkowitz, K. B.; Boyd, D. B., Eds. VCH Publishing: New York, 1991; Vol. 2, pp 313−366.
(27) Van der Pol, C.; Bryce, M. R.; Wielopolski, M.; Atienza-Castellanos, C.; Dirk, M.; Guldi, D. M.; Filippone, S.; Martín, N. Energy Transfer in Oligofluorene-C_{60} and C_{60}-Oligofluorene-C_{60} Donor−Acceptor Conjugates. *J. Org. Chem.* **2007**, *72*, 6662−6671.
(28) Lin, T.-C.; Huang, Y.-J.; Chen, Y.-F.; Hu, C.-L. Two-Photon Absorption and Effective Broadband Optical Power Limiting Properties of a Multi-Branched Chromophore Containing 2,3-Diarylquinoxalinyl Moieties as the Electron-Pulling Units. *Tetrahedron* **2010**, *66*, 1375−1382.
(29) Lakowicz, J. R. *Principles of Fluorescence Spectroscopy*; Kluwer Academic Publishers: New York, 1999.
(30) Reynolds, G. A.; Drexhage, K. H. New Coumarin Dyes with Rigidized Structure for Flashlamp-Pumped Dye Lasers. *Opt. Commun.* **1975**, *13*, 222−225.
(31) Corredor, C. C.; Belfield, K. D.; Bondar, M. V.; Przhonska, O. V.; Yao, S. One- and Two-Photon Photochemical Stability of Linear and Branched Fluorene Derivatives. *J. Photochem. Photobiol. A* **2006**, *184*, 105−112.
(32) Belfield, K. D.; Bondar, M. V.; Morales, A. R.; Yue, X.; Luchita, G.; Przhonska, O. V.; Kachkovsky, O. D. Two-Photon Absorption and Time-Resolved Stimulated Emission Depletion Spectroscopy of a New Fluorenyl Derivative. *ChemPhysChem* **2012**, *13*, 3481−3491.
(33) Belfield, K. D.; Bondar, M. V.; Morales, A. R.; Yue, X.; Luchita, G.; Przhonska, O. V. Transient Excited-State Absorption and Gain Spectroscopy of a Two-Photon Absorbing Probe with Efficient Superfluorescent Properties. *J. Phys. Chem. C* **2012**, *116*, 11261−11271.
(34) Sheik-Bahae, M.; Said, A. A.; Wei, T. H.; Hagan, D. J.; Van Stryland, E. W. Sensitive Measurement of Optical Nonlinearities Using a Single Beam. *IEEE J. Quantum Elect.* **1990**, *26*, 760−769.
(35) Lepkowicz, R. S.; Przhonska, O. V.; Hales, J. M.; Hagan, D. J.; Van Stryland, E. W.; Bondar, M. V.; Slominsky, Y. L.; Kachkovski, A. D. Excited-State Absorption Dynamics in Polymethine Dyes Detected by Polarization-Resolved Pump-Probe Measurements. *Chem. Phys.* **2003**, *286*, 277−291.
(36) Frisch, M. J.; Trucks, G. W.; Schlegel, H. B.; Scuseria, G. E.; Robb, M. A.; Cheeseman, J. R.; Scalmani, G.; Barone, V.; Mennucci, B.; Petersson, G. A.; Nakatsuji, H.; Caricato, M.; Li, X.; Hratchian, H. P.; Izmaylov, A. F.; Bloino, J.; Zheng, G.; Sonnenberg, J. L.; Hada, M.; Ehara, M.; Toyota, K.; Fukuda, R.; Hasegawa, J.; Ishida, M.; Nakajima, T.; Honda, Y.; Kitao, O.; Nakai, H.; Vreven, T.; Montgomery, J. J. A.; Peralta, J. E.; Ogliaro, F.; Bearpark, M.; Heyd, J. J.; Brothers, E.; Kudin, K. N.; Staroverov, V. N.; Kobayashi, R.; Normand, J.; Raghavachari, K.; Rendell, A.; Burant, J. C.; Iyengar, S. S.; Tomasi, J.; Cossi, M.; Rega, N.; Millam, N. J.; Klene, M.; Knox, J. E.; Cross, J. B.; Bakken, V.; Adamo, C.; Jaramillo, J.; Gomperts, R.; Stratmann, R. E.; Yazyev, O.; Austin, A. J.; Cammi, R.; Pomelli, C.; Ochterski, J. W.; Martin, R. L.; Morokuma, K.; Zakrzewski, V. G.; Voth, G. A.; Salvador, P.; Dannenberg, J. J.; Dapprich, S.; Daniels, A. D.; Farkas, Ö.; Foresman, J. B.; Ortiz, J. V.; Cioslowski, J.; Fox, D. J. *Gaussian 09*, Revision A.2; Gaussian, Inc.: Wallingford, CT, 2009.
(37) Stephens, P. J.; Devlin, F. J.; Chabalowski, C. F.; Frisch, M. J. Ab Initio Calculation of Vibrational Absorption and Circular Dichroism Spectra Using Density Functional Force Fields. *J. Phys. Chem.* **1994**, *98*, 11623−11627.
(38) Hehre, W. J.; Ditchfield, R.; Pople, J. A. Self-Consistent Molecular Orbital Methods. XII. Further Extensions of Gaussian-Type Basis Sets for Use in Molecular Orbital Studies of Organic Molecules. *J. Chem. Phys.* **1972**, *56*, 2257−2261.
(39) Yanai, T.; Tew, D. P.; Handy, N. C. A New Hybrid Exchange-Correlation Functional Using the Coulomb-Attenuating Method (Cam-B3LYP). *Chem. Phys. Lett.* **2004**, *393*, 51−57.
(40) Mikhailov, I. A.; Bondar, M. V.; Belfield, K. D.; Masunov, A. E. Electronic Properties of a New Two-Photon Absorbing Fluorene Derivative: The Role of Hartree-Fock Exchange in the Density Functional Theory Design of Improved Nonlinear Chromophores. *J. Phys. Chem. C* **2009**, *113*, 20719−20724.
(41) Masunov, A.; Tretiak, S. Prediction of Two-Photon Absorption Properties for Organic Chromophores Using Time-Dependent Density- Functional Theory. *J. Phys. Chem. B* **2004**, *108*, 899−907.
(42) Nelson, T.; Fernandez-Alberti, S.; Chernyak, V.; Roitberg, A. E.; Tretiak, S. Nonadiabatic Excited-State Molecular Dynamics Modeling of Photoinduced Dynamics in Conjugated Molecules. *J. Phys. Chem. B* **2011**, *115*, 5402−5414.
(43) Ohta, K.; Antonov, L.; Yamada, S.; Kamada, K. Theoretical Study of the Two-Photon Absorption Properties of Several Asymmetrically Substituted Stilbenoid Molecules. *J. Chem. Phys.* **2007**, *127*, 084504/1−12.
(44) Martin, R. L. Natural Transition Orbitals. *J. Chem. Phys.* **2003**, *118*, 4775−4777.
(45) Seedher, N.; Kanojia, M. Mechanism of Interaction of Hypoglycemic Agents Glimepiride and Glipizide with Human Serum Albumin. *Cent. Eur. J. Chem.* **2009**, *7*, 96−104.
(46) Seedher, N.; Agarwal, P. Competitive Binding of Fluoroquinolone Antibiotics and Some Other Drugs to Human Serum Albumin: A Luminescence Spectroscopic Study. *Luminescence* **2013**, *28*, 562−568.
(47) Meier, H.; Petermann, R.; Gerold, J. Bathochromic or Hypsochromic Effects Via the Extension of Conjugation: A Study of Stilbenoid Squaraines. *Chem. Commun.* **1999**, 977−978.

DOI: 10.1021/am508093p
ACS Appl. Mater. Interfaces 2015, 7, 2833−2846

(48) Szemik-Hojniak, A.; Balkowski, G. J.; Wurpel, G. W. H.; Jurek Herbich, J.; van der Waals, J. H.; Buma, W. J. Photophysics of 1,8-Bis(dimethylamino)naphthalene in Solution: Internal Charge Transfer with a Twist. *J. Phys. Chem. A* **2004**, *108*, 10623−10631.
(49) Lemaster, J. J.; Trollinger, D. R.; Qian, T.; Cascio, W. E.; Ohata, H. Confocal Imaging of Ca^{2+}, Ph, Electrical Potential, and Membrane Permeability in Single Living Cells. *Method. Enzymol.* **1999**, *302*, 341−356.
(50) Belfield, K. D.; Bondar, M. V.; Kachkovsky, O. D.; Przhonska, O. V.; Yao, S. Solvent Effect on the Steady-State Fluorescence Anisotropy of Two-Photon Absorbing Fluorene Derivatives. *J. Lumin.* **2007**, *126*, 14−20.
(51) Belfield, K. D.; Bondar, M. V.; Hernandezt, F. E.; Przhonska, O. V.; Yao, S. Two-Photon Absorption Cross Section Determination for Fluorene Derivatives: Analysis of the Methodology and Elucidation of the Origin of the Absorption Processes. *J. Phys. Chem. B* **2007**, *111*, 12723−12729.
(52) Belfield, K. D.; Bondar, M. V.; Corredor, C. C.; Hernandez, F. E.; Przhonska, O. V.; Yao, S. Two-Photon Photochromism of a Diarylethene Enhanced by Ferster Resonance Energy Transfer from Two-Photon Absorbing Fluorenes. *ChemPhysChem* **2006**, *7*, 2514−2519.
(53) Terenziani, F.; Painelli, A.; Katan, C.; Charlot, M.; Blanchard-Desce, M. Charge Instability in Quadrupolar Chromophores: Symmetry Breaking and Solvatochromism. *J. Am. Chem. Soc.* **2006**, *128*, 15742−15755.
(54) Belfield, K. D.; Bondar, M. V.; Morales, A. R.; Padilha, L. A.; Przhonska, O. V.; Wang, X. Two-Photon STED Spectral Determination for a New V-Shaped Organic Fluorescent Probe with Efficient Two-Photon Absorption. *ChemPhysChem* **2011**, *12*, 2755−2762.
(55) Wang, X.; Yao, S.; Ahn, H.-Y.; Zhang, Y.; Bondar, M. V.; Torres, J. A.; Belfield, K. D. Folate Receptor Targeting Silica Nanoparticle Probe for Two-Photon Fluorescence Bioimaging. *Biomed. Opt. Express* **2010**, *1*, 453−462.
(56) Wang, X.; Nguyen, D. M.; Yanez, C. O.; Rodriguez, L.; Ahn, H.-Y.; Bondar, M. V.; Belfield, K. D. High-Fidelity Hydrophilic Probe for Two-Photon Fluorescence Lysosomal Imaging. *J. Am. Chem. Soc.* **2010**, *132*, 12237−12239.
(57) Efimova, S. L.; Malyukin, Y. V. Franck-Condon State Relaxation in Some Pyrazoline Luminophor. *Funct. Mater.* **2002**, *9*, 247−250.
(58) Pozdnyakov, I. P.; Kolomeets, A. V.; Plyusnin, V. F.; Melnikov, A. A.; Kompanets, V. O.; Chekalin, S. V.; Tkachenko, N.; Lemmetyinen, H. Photophysics of Fe(III)−Tartrate and Fe(III)−Citrate Complexes in Aqueous Solutions. *Chem. Phys. Lett.* **2012**, *530*, 45−48.
(59) Faulhaber, K.; Granzhan, A.; Ihmels, H.; Otto, D.; Thomas, L.; Wells, S. Studies of the Fluorescence Light-up Effect of Amino-Substituted Benzo[b]quinolizinium Derivatives in the Presence of Biomacromolecules. *Photochem. Photobiol. Sci.* **2011**, *10*, 1535−1545.
(60) Khan, A. Y.; Hossain, M.; Kumar, G. S. Binding of Plant Alkaloids Berberine and Palmatine to Serum Albumins: A Thermodynamic Investigation. *Mol. Biol. Rep.* **2013**, *40*, 553−566.
(61) Abou-Zied, O. K.; Al-Shihi, O. I. K. Characterization of Subdomain IIA Binding Site of Human Serum Albumin in Its Native, Unfolded, and Refolded States Using Small Molecular Probes. *J. Am. Chem. Soc.* **2008**, *130*, 10793−10801.
(62) Khan, A. Y.; Hossain, M.; Kumar, G. S. Binding of Plant Alkaloids Berberine and Palmatine to Serum Albumins: A Thermodynamic Investigation. *Mol. Biol. Rep.* **2013**, *40*, 553−566.
(63) Chang, K. J.; Bennett, V.; Cuatrecasas, P. Membrane Receptors as General Markers for Plasma-Membrane Isolation Procedures—Use of I-125-Labeled Wheat-Germ Agglutinin, Insulin, and Cholera Toxin. *J. Biol. Chem.* **1975**, *250*, 488−500.

DOI: 10.1021/am508093p
ACS Appl. Mater. Interfaces 2015, 7, 2833−2846